Author's Response

Reviewer #1

Comment: Specifically, authors used magnetic methods to quantify the magnetic particles, but they only measured χ and χ_{fd}. χ is affected by many factors, e.g., concentration, grain size, mineral types.The current study focused only on concentration without information of grain size and mineral types. I strongly encourage authors to provide a more comprehensive study on this issue.

Reply: Thanks for this comment. We conducted more magnetic measurements (see Method section, Lines 11-23 in Page 5 in the revised version). The temperature dependent susceptibility (χ-T), hyteresis loops and first-order reversal curves (FORC) were used to better constrain the grain size and types of magnetic minerals (see Figs. 3 and 4, Lines 10-22 in Page 6 and Lines 1-5 in Page 7 in the revised version).

χ-T is used to identify magnetic mineral composition. All the χ-T heating curves (Fig. 3a-f) are characterized by a major susceptibility decrease at 580 ℃, i.e. the Curie temperature of magnetite, which pinpoint magnetite as the major contributor to χ. All the samples are irreversible with cooling paths above heating trajectories due to the neoformation of magnetite (Jordanova et al., 2004; Kim et al., 2009). The χ-T heating curves of the vehicle exhausts displays a decreasing χ between 580 and 700 ℃ (Fig. 3b), suggesting the presence of hematite.

All samples have similar slightly wasp-waisted hysteresis loops (Fig. 3g-l). Their magnetic saturation was generally reached at a magnetic field of about 300 mT. This is a clear indication of the predominance of low coercivity ferrimagnetic minerals in all samples.

The Day plot and FORC diagram are powerful methods to identify the domain state distribution of magnetic materials (Day et al., 1977; Dunlop 2002a, b; Pike et al., 1999; Roberts et al., 2000; Harrison et al., 2008). All the samples agree well with single-domain (SD) + multi-domain (MD) admixture curves in the pseudo-single-domain (PSD) range of the Day plot (Fig. 4a). The FORC diagrams for street dust (Fig. 4d), and anthropogenic pollutant (Fig. 4e) have divergent contours that are characteristic of MD grains. The FORC diagram for natural surface sediments seems to be characteristic of PSD/MD behavior, whose outer contours display divergent pattern and inner contours are somewhat less divergent (Fig. 4a). The FORC distributions of atmospheric dustfall (Fig. 4b) appear to have a mixed set of contours. The outer contours have a divergent pattern that would be expected for MD particles, while the inner contours close about a central peak represent SD grains.

Day, R., Fuller, M., Schmidt, V.A.: Hysteresis properties of titanomagnetites: grain-size and compositional dependence. Phys Earth Planet Inter., 13, 260-267,1977.

Dunlop, D. J.: Theory and application of the Day plot (Mrs/Ms versus Hcr/Hc) 1. Theoretical curves and tests using titanomagnetite data, J. Geophys. Res., 107, 2076, https://doi.org/10.1029/2001jb000486, 2002a.

Dunlop, D. J.: Theory and application of the Day plot (Mrs/Ms versus Hcr/Hc) 2. Application to data for rocks, sediments, and soils, J. Geophys. Res., 107, 2057, https://doi.org/10.1029/2001jb000487, 2002b.

Harrison, R. J., Feinberg, J. M.: FORCinel: An improved algorithm for calculating first-order reversal curve distributions using locally weighted regression smoothing, Geochem. Geophys. Geosyst., 9, Q05016, https://doi.org/10.1029/2008GC001987, 2008.

Jordanova, D., Hoffmann, V., and Febr, K. T.: Mineralmagnetic characterization of anthropogenic magnetic phases in the Danube river sediments (Bulgarian part), Earth planet. Sci. Lett., 30, 71-89, https://doi.org/10.1016/S0012-821X(04)00074-3, 2004.

Kim, W., Doh, S. J., and Yu, Y. J.: Anthropogenic contribution of magnetic particulates in urban roadside dust, Atmos. Environ., 43, 3137-3144, https://doi.org/10.1016/j.atmosenv.2009.02.056, 2009.

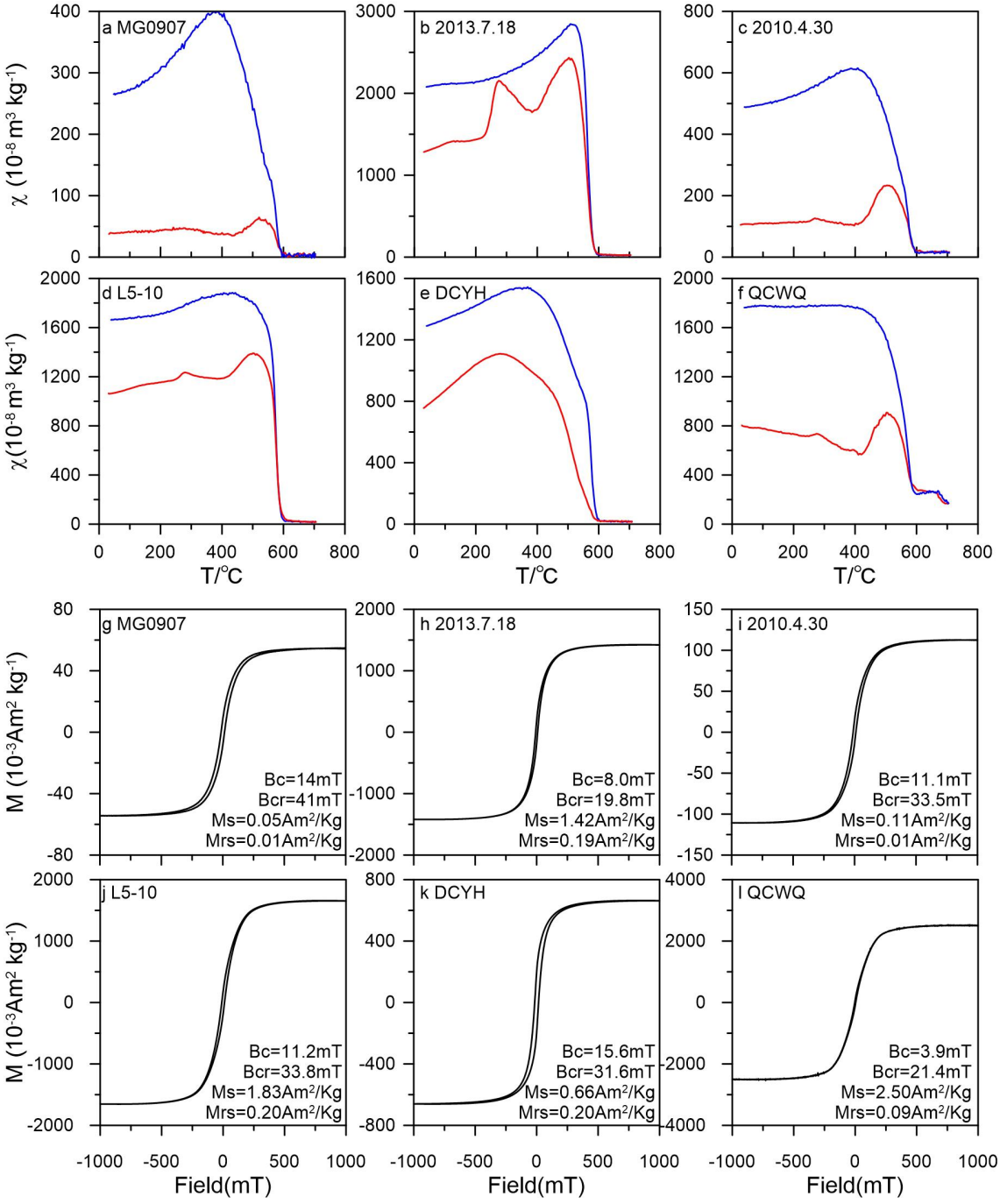

Fig 3. χ-T heating (red line) and cooling (blue line) curves (a-f) and magnetic hysteresis loops (g-l) of representative samples of NSS (MG0907), atmospheric dustfall (AD, 2013.7.18 and 2010.4.30), street dust (STD, L5-10) and anthropogenic pollutant (AP): fly ashes (DCYH) and vehicle exhausts (QCWQ).

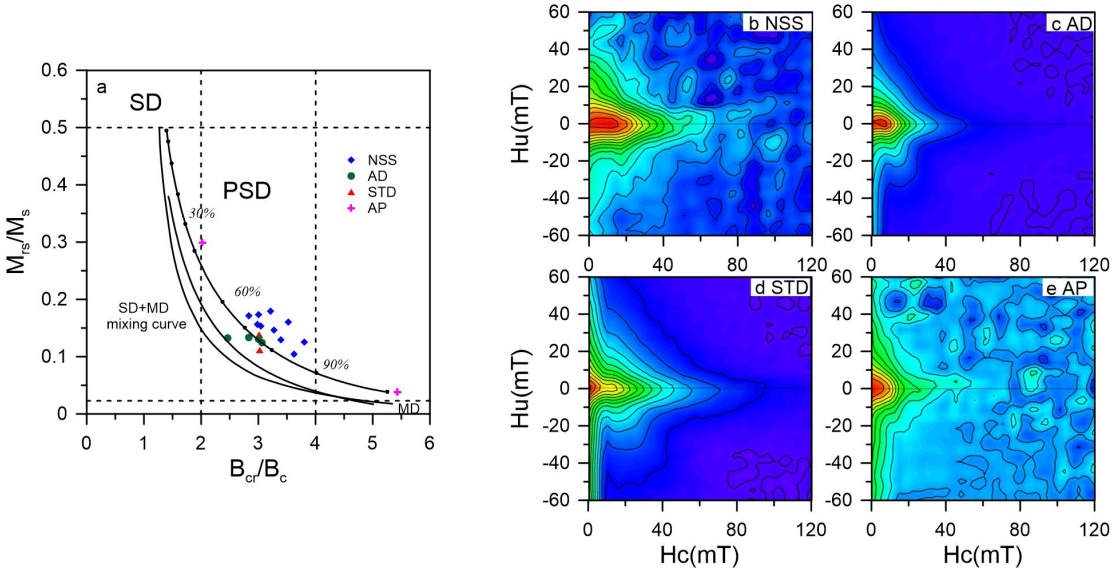

Fig. 4 (a) Day-plot of the ratios M_{rs}/M_s and B_{cr}/B_c for representative samples from NSS, AD, STD, and AP, grain size boundaries and the SD+MD matrix line are according to Dunlop (2002). Percentages in the Day plot represent the concentrations of MD in the SD+MD mixture; (b-e) FORC diagrams for representative samples of NSS, AD, STD, and AP.

Reviewer #2

Major points:

1. Comment: Authors mainly applied magnetic susceptibility to resolve the natural and anthropogenic signitures. Because χ_{lf} and χ_{fd} can be controlled by various factors including mineralogy and grain-size, more detailed magnetic data should greatly improve the quality of this paper.

Reply: Thanks for your suggestion. We added more magnetic measurements to assess the grain size and mineral type (see a detailed response to the first reviewer's comment).

2. **Comment:** Such a qualitative result may be estimated only by dustflux ratio without χ_{lf} data. To clarify the discussion 4.1, authors are highly encouraged to present quantitative magnetic data such as a saturation magnetization.

Reply: To clarify the discussion 4.1, we used the method of running median (Härdle and Steiger, 1995; Zhen and Yan, 1988; Marron, 1987; Mudelsee, 2006) to estimate the background of the observed weekly dust flux (see Fig. 10a, Lines 8-18 in Page 10 in the revised version) and then calculate monthly local anthropogenic contributions LC_{flux} by ratio of monthly local background and total dust flux (see Fig. 10a, Lines 19-22 in Page 10 and lines 1-2 in Page 11 in the revised version).

Saturation magnetization (M_s) of representative samples (Fig.3h-m) were measured to identify concentration of ferrimagnetic minerals. We found that the averaged values of M_s in different sources show a rising trend from the natural surface sediments (0.04 Am^2/kg) to atmospheric dustfall (0.81 Am^2/kg) and street dust (1.03 Am^2/kg), and then to anthropogenic pollutant (1.58 Am^2/kg), which correspond to the characteristics of averaged χ_{lf} in different sources. This indicates that the high χ_{lf} of urban dust is caused by the ferrimagnetic mineral from local anthropogenic source. In consequence, the LC contribution could also be estimated by the average χ_{lf} (25×10^{-8} m^3 kg^{-1}) of the surface sediments and local street dust (550×10^{-8} m^3 kg^{-1}). On this basis, we calculated the LC_{χ} (see Fig.10b, Lines 3-12 in 11 Page in the revised version).

The result showed that LC_{flux} and LC_{χ} values have the same trend and show a distinctive seasonal pattern (Fig. 10a-b), with the maximum in autumn (92.4 %, 92.3%), followed by winter (90.8 %, 74.7 %), summer (83.5 %, 71 %), and spring (73.0 %, 53.1%). Both the LC_{flux} and LC_{χ} are the lowest in spring, implying that distant natural dust input makes a great contribution to atmospheric dustfall during this period (see Fig.10a-b, Lines13-16 in Page 11 in the revised version). *The LC variation exhibits a similar seasonal pattern with χ_{lf}, but opposite trend to that of dust flux (Fig. 10a-b). This means that dominant anthropogenic magnetic signals were diluted by less magnetic natural dust input. Hence, the local contribution is reduced as a result of increasing natural dust flux in spring* (see Fig.10a-b, Lines1-4 in Page 14 in the revised version)..

Minor points

1. Comment: Figure 1: Insert a scale bar in a road-map.

Reply: We inserted a scale bar in the top left corner of road-map in Fig.1 (see Fig. 1b).

2. Comment: Page 3, line 6: Check the reference (Maher et al., 1988)

Reply: We checked the reference and deleted it.

3. Comment: Page 4, line 18: Sampling time? Fitering? Dust bag? Not enough information for sampling.

Reply: We added description on sampling time. The sample of fly ashes were taken from dust bag of electrostatic precipitators at the Baqiao thermal power plant (see Lines 16-21 in Page 4 in the revised version).

4. Comment: Page 6, lines 10 and 11: Why χ_{lf} indicates different mineralogy?

Reply: We corrected this sentence to "*The different distribution patterns of χ_{lf} indicate that the assemblage of magnetic minerals in the NCD and TD may different from those in the MG and TP*" (see Lines 18-19 in Page 7 in the revised version).

5. Comment: Page 6, line 15: Difference in mean χ_{fd} values of 6.9%, 5.1%, 4.6%, and 2.5% have any scientific meaning?

Reply: *χ_{fd} is sensitive to the superparamagnetic (SP) component. There are virtually no SP grains when χ_{fd} is < 2 %, while a mixture of SP and coarser grains is indicated with χ_{fd} in the range of 2-10% (Dearing et al. 1994)* (see Lines 9-11 in Page 7).

6. Comment: Page 7, line 13: Is that platinum or carbon coat for SEM observation?

Reply: *Samples were mounted on SEM stub with the double-sided carbon tape and then coated with thin gold film* (see Lines 4-5 in Page 6).

Härdle, W., Steiger, W.: Algorithm AS 296: Optimal median smoothing, Journal of the Royal Statistical Society. Series C (Applied Statistics)., 44, 258-264, 1995.

Marron, J. S.: What does Optimal Bandwidth Selection Mean for Nonparametric Regression Estimation?., Department of Statistics, University of North Carolina at Chapel Hill, 1986.

Mudelsee, M.: Short note: CLIM-X-DETECT: A Fortran 90 program for robust detection of extremes against a time-dependent background in climate records, Computers & Geosciences., 32, 141-144, https://doi.org/10.1016/j.cageo.2005.05.010, 2006.

Zheng, Z. G., Yang, Y.: Cross-validation and median criterion, Statistica Sinica., 8 , 907-921, 1998.

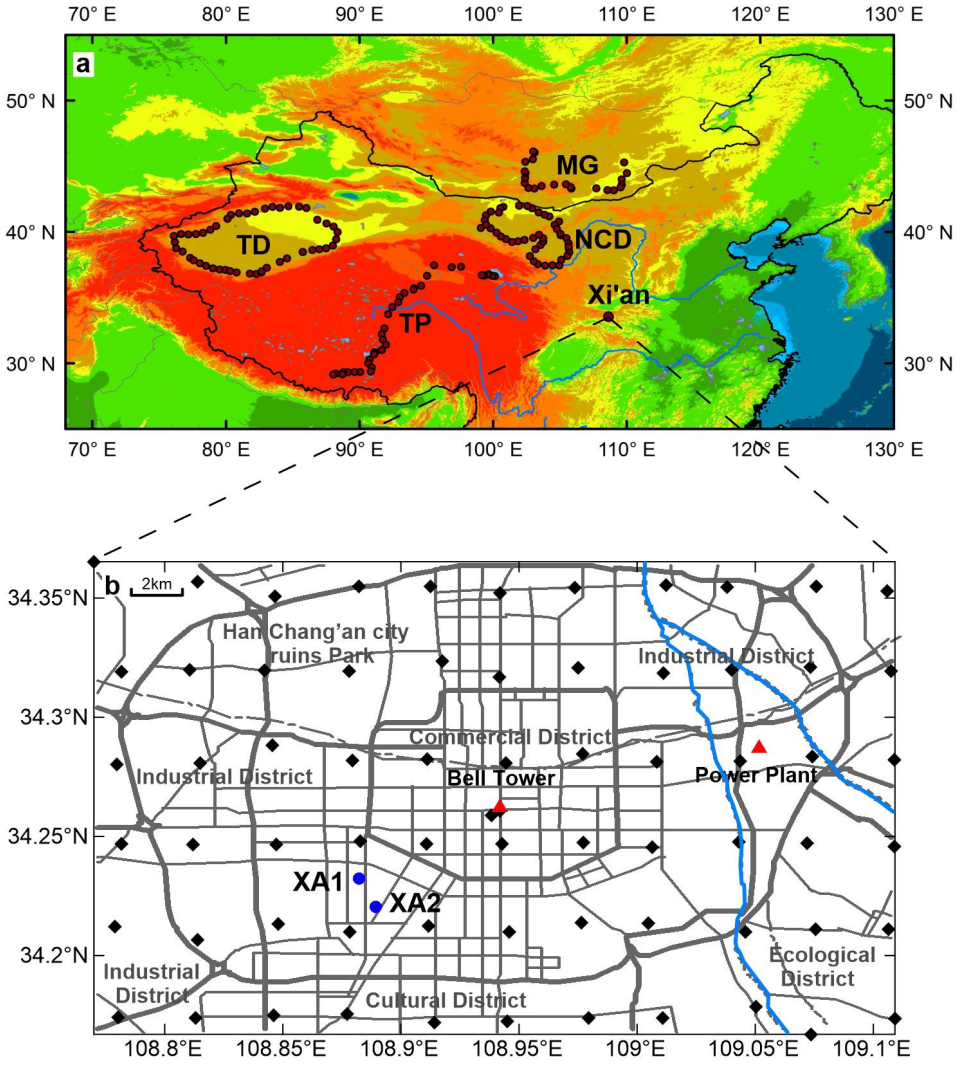

Figure 1. Locations of natural surface sediments (NSS) in the East Asian sources (a) and urban dust samples in Xi'an (b). NCD - northern Chinese deserts, MG - Mongolian Gobi, TD - Taklimakan Desert, and TP - Tibetan Plateau. Black diamonds are STD sampling sites; blue dots are samples of consecutive AD (XA1 at the Institute of Earth Environment, Chinese Academy of Sciences; XA2 at the Xinxinjiayuan residential community); red triangles are typical heavily-polluted sites, including the Bell Tower in an area of high traffic density, and the Baqiao thermal power plant.

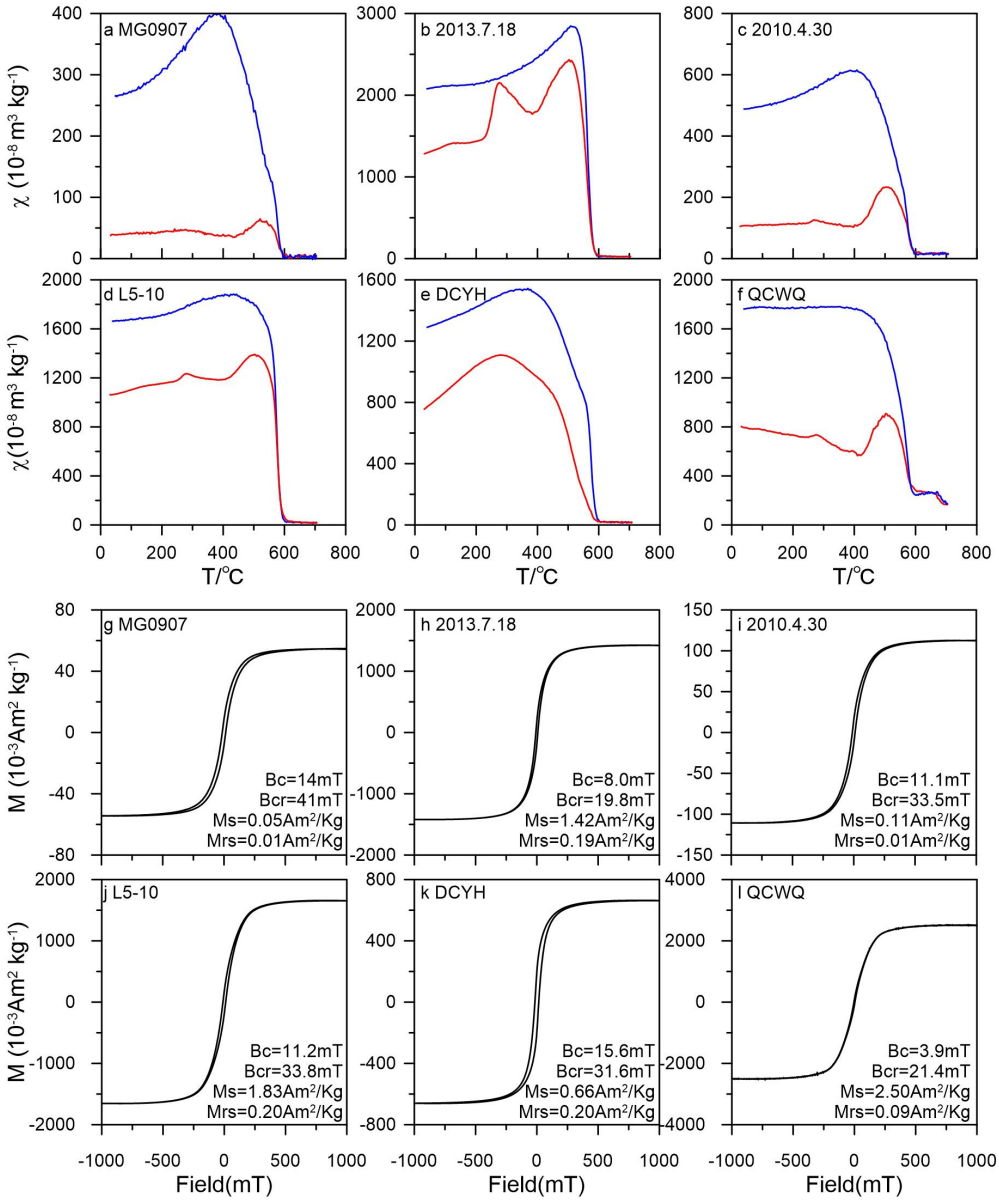

Fig 3. χ-T heating (red line) and cooling (blue line) curves (a-f) and magnetic hysteresis loops (g-l) of representative samples of NSS (MG0907), atmospheric dustfall (AD, 2013.7.18 and 2010.4.30), street dust (STD, L5-10) and anthropogenic pollutant (AP): fly ashes(DCYH) and vehicle exhausts (QCWQ).

5

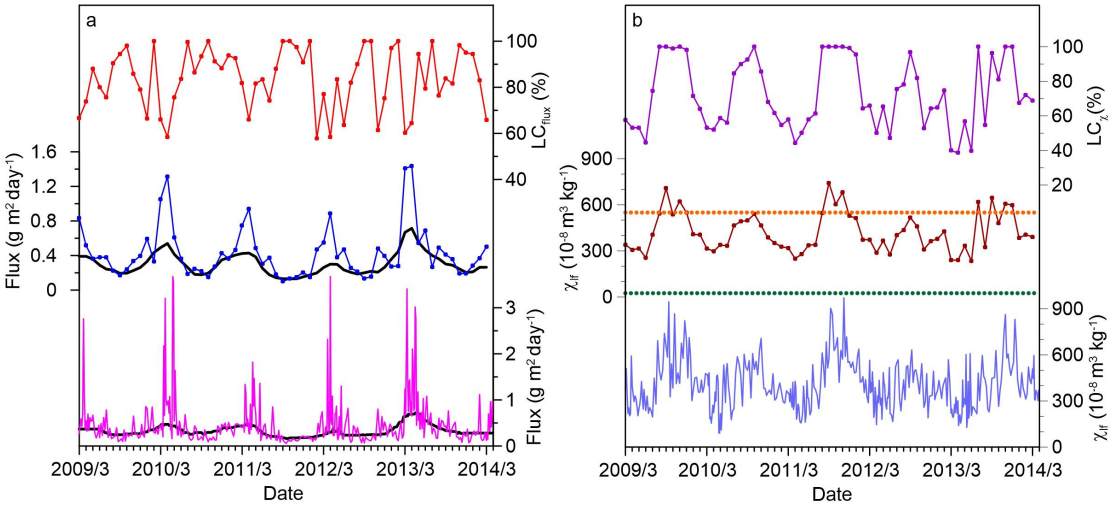

Fig. 10 The estimated local anthropogenic contributions by dust flux (a) and χ_{lf} (b). From bottom to top: (a) weekly dust flux (pink) and background estimate by the running median with a cross-validated number of window points (k=19) (black), monthly averaged dust flux (blue) and background (black), local contribution (red) estimate by dust flux at XA1; (b) weekly χ_{lf} values (light blue), averaged χ_{lf} values of natural distant dust (green dotted lines), monthly averaged χ_{lf} values (brown), averaged χ_{lf} values of local street dust (orange dotted lines) , local contribution (violet) estimate by χ_{lf} at XA1.

Magnetic signatures of natural and anthropogenic sources of urban dust aerosol

Haijiao Liu[1,2], Yan Yan[3], Hong Chang[1], Hongyun Chen[4], Lianji Liang[5], Xingxing Liu[1], Xiaoke Qiang[1], Youbin Sun[1,6]

[1]State Key Laboratory of Loess and Quaternary Geology, Institute of Earth Environment, Chinese Academy of Sciences, Xi'an, 710061, China

[2]College of Earth Science, University of Chinese Academy of Sciences, Beijing, 100049, China

[3]Guangzhou Institute of Geochemistry, Chinese Academy of Sciences, Guangzhou, 510640, China

[4]Research Center for Loess and Global Changes, Institute of Hydrogeology and Environmental Geology, Chinese Academy of Geological Sciences, Shijiazhuang, 050803, China

[5]College of Architecture and Civil Engineering, Beijing University of Technology, Beijing, 100124, China

[6]Institute of Global Environmental Change, Xi'an Jiaotong University, Xi'an, 710049, China

Corresponding to: Youbin Sun (sunyb@ieecas.cn)

Abstract. The characteristics of urban dust aerosols and the contributions of their natural and anthropogenic sources are of scientific interests as well as being of substantial sociopolitical and economic concerns. Here we present a comprehensive study of dust flux, magnetic parameters, and magnetic particulates' morphology and elemental composition of atmospheric dustfall originating from natural dust sources in East Asia and local anthropogenic sources in Xi'an, China. The results reveal a significant seasonally inverse relationship between variations of dust flux and magnetic susceptibility (χ). By comparing dust flux and χ records, the relative contributions of dust from local anthropogenic sources are estimated. Analyses using Scanning Electron Microscopy (SEM) combined with Energy Dispersive Spectroscopy (EDS) indicate that magnetic particulates from different sources have distinctive morphological and elemental characteristics. Detrital magnetic particles originating from natural sources are characterized by relatively smooth surfaces with Fe and O as the major elements and a minor contribution from Ti. The anthropogenic particles have angular, spherical, aggregate, and porous shapes with distinctive contributions from marker elements, including S, Cr, Cu, Zn, Ni, Mn and Ca. Our results demonstrate that this multidisciplinary approach is effective in distinguishing dust derived from distant natural sources and local

anthropogenic sources, and for quantitative assessment of contributions from the two end-members.

1 Introduction

Urban dust aerosols, comprising of both natural and anthropogenic contributions with complex morphological and physiochemical characteristics, have become a focus of studies of global climate change and regional air pollution (Wilson et al., 2002). Natural dust is derived primarily from long-range transport with a minor local soil contribution, which often causes dust events including sandstorm, suspended-dust and blown-sand weathers (Sun et al., 2001; Zhang et al., 2003a; Chen et al., 2004; Kan et al., 2007; Baddock et al., 2013), and has a deleterious effect on local air quality (Wang et al., 2004; Ginoux et al., 2004). Anthropogenic dust produced by human activities is characterized by high concentrations of toxic heavy metals (e.g., Pb, Zn, Co, Cr, Ni, As), which has a long-lasting and more adverse impact on local environment and human health (Zdanovicz et al., 2006; Qiao et al., 2013; Lu et al., 2014; Lee et al., 2015).

Airborne particulate matter < 2.5 μm in diameter (e.g., PM2.5 and PM1) can enter the alveolar region and blood circulatory system leading to health issues and even death (Brunekreef, et al., 2002; Nel et al., 2006; Pickrell et al., 2009; Maher et al., 2013). Moreover, anthropogenic dust is an important medium for the formation of secondary pollutants and plays a significant role in the formation of haze events (Hanisch and Crowley, 2001; Li et al., 2001; Lee et al., 2002; Usher et al., 2002; Finlayson-Pitts et al., 2003; Rubasinghege and Grassian, 2009; Takeuchi et al., 2010; Wu et al., 2011; Huang et al., 2014). Consequently, it is important to distinguish the characteristics and contributions of natural and anthropogenic dust in urban aerosols to formulate effective policies for city administrations on abating dust pollution and improving atmospheric environment.

Natural and anthropogenic contributions to urban dust aerosols are usually assessed quantitatively using geochemical and magnetic methodologies (Gorden, 1988; Xie et al., 1999; Gomez et al., 2004; Spassov et al., 2004; Kim et al., 2009; Feng et al., 2012). Geochemical methods typically involve source apportionment and contribution assessment of representative heavy metal elements using statistical methods such as chemical mass balance (CMB) (Chow et al., 2002; Gupta et al., 2006) and factor analysis (FA) (Harrison et al., 1997a; Salvador et al., 2004). According to their sensitivity to various

anthropogenic factors, Pb, Fe, Zn, Cr, Cd, Ni, Ba and Sb were frequently used as marker elements for vehicle emissions (Huang et al., 1994; Adachi et al., 2004; Meza-Figueroa et al., 2007), while Hg, Pb, Mn, Cr, Co, Cu, Cd and Ni were regarded indicative of coal-combustion contribution (Vouk and Piver, 1983; Pacyna and Pacyna , 2001; Sushil and Batra., 2006).

Since magnetic measurements are rapid, inexpensive and non-destructive, environmental magnetism is increasingly being used as an effective approach to study urban dust pollution (Hoffmann et al., 1999; Maher et al., 1998). By combining magnetic properties with morphological (Muxworthy et al., 2001; Urbat et al., 2004; Blaha et al., 2008a), heavy metal (Hunt et al., 1984; de Miguel et al., 1997; Blaha et al., 2008b; Maher et al., 2008), and back trajectory characteristics (Li et al., 2009; Wehner et al., 2008; Fleming et al., 2012), the provenance, transport routes and spatial distribution of polluted dust aerosols can be investigated. This multidisciplinary approach is becoming a popular means of urban pollution monitoring and assessment (Jordanova et al., 2014; Stein et al., 2015; Yan et al., 2015; Bourliva et al., 2016).

Using environmental magnetic techniques to assess pollution levels and sources, different forms of urban dust aerosols in East Asia have been studied, including atmospheric dustfall, street dust, leaf dust, inhalable particulate matter, and surface soil. For example, spatial and temporal pollution patterns were quantitatively estimated from seasonal fluctuations of the concentration and grain-size of magnetic particles in urban roadside dust (Kim et al., 2007, 2009). A high correlation between magnetic parameters (magnetic susceptibility and saturation isothermal remanence, i.e. χ and SIRM) and heavy metal concentrations in street dust, polluted farmland soil and atmospheric dustfall was observed, indicating that these magnetic parameters can be employed as effective proxies to assess heavy metal pollution (Zhang et al., 2011, 2012a, b; Qiao et al., 2013). SIRM characteristics of roadside leaves were proven a reflection of spatial variations of magnetic particles in urban dustfall (Hansard et al., 2011, 2012; Quayle et al., 2010; Maher et al., 2013; Kardel et al., 2012). Although morphology, grain-size, mineral and element analyses were utilized in previous works, there lacks studies presenting a systematic source-to-sink comparison among magnetic signatures of natural dust, urban dust aerosol, and polluted dust.

This study systematically collected surface sediments from potential dust sources in East Asia, urban dust aerosols in Xi'an, including atmospheric dustfall (consecutive over five years) and street dust, and typical anthropogenic pollutants such

as vehicle exhausts and fly ashes. Morphology and elemental compositions of magnetic particles in representative samples were analyzed to facilitate a thorough source-sink comparison. Our results indicate that natural and anthropogenic contributions to urban dust aerosols can be differentiated using a combination of their magnetic, morphological and elemental characteristics.

2 Sampling and methods

2.1 Sampling

Surface sediments were collected in potential dust sources of East Asia, including the northern Chinese deserts (NCD, including the Badain Juran and Tengger Deserts), Taklimakan Desert (TD), Mongolian Gobi (MG) and Tibetan Plateau (TP) (Fig. 1a). Fine-grained materials were taken from alluvial fans, dry riverbeds, lake basins, and drainage depressions within Gobi/sandy deserts at intervals of 100 to 200 km (Fig. 2a-d). To better understand the different sedimentary characteristics, 48 samples from the NCD, 50 samples from the TD, 23 samples from the MG, and 32 samples from the TP were selected for measurement. Locations of the samples are shown in Fig. 1. Detailed descriptions were given in Sun et al., (2013).

Sixty-eight street dust samples were collected from parks, construction sites, commercial streets, and residential areas in Xi'an following a 3×4 km grid spanning approximately 30 km from west to east, and 20 km from north to south (Fig. 1b). The sampling grid covers a range of different functional areas in Xi'an, including the Industrial District, Commercial District, Cultural District, Ecological District, and Han Chang'an city ruins Park (Fig. 1b). We also collected four typical anthropogenic pollutant samples in June 2017, including one sample of vehicle exhausts from the exhaust pipes of several vehicles, one sample of fly ashes from dust bag of electrostatic precipitators at the Baqiao thermal power plant, one street dust sample from the Bell Tower in downtown Xi'an which experiences daily traffic jams, and one street dust sample near the Baqiao thermal power plant where coal-burning is the leading pollution factor. The locations of these samples are shown in Fig. 1.

Atmospheric dustfall collectors were placed on the top of a four-story building at the Institute of Earth Environment, Chinese Academy of Sciences, ~10 m above the ground surface, and a 15-story building inside the Xinxinjiayuan residential

community, ~50 m above the ground surface (Fig. 2e-f). The sampling sites situated in southwest Xi'an consist primarily of commercial and residential districts. Samples were collected using the wet-collection method (Qian and Dong, 2004) at time intervals of 3-5 days in spring and 6-7 days in other seasons. Detailed sampling procedures were reported by Yan et al. (2015a, b). 733 samples were collected from March 2009 to March 2014. Dust flux (DF, g m^{-2} day^{-1}) is calculated as follows:

$$DF=W/(A\times T), \quad (1)$$

where W is the sample weight in g, A is the area in m^2, and T is time in day.

2.2 Methods

Low- and high-frequency magnetic susceptibilities (χ_{lf} and χ_{hf}, respectively) were measured using a MFK1-FA Kappabridge at frequencies of 976 Hz and 15,616 Hz. Frequency-dependent magnetic susceptibility (χ_{fd}) was calculated as $(\chi_{lf} - \chi_{hf}) / \chi_{lf} \times 100\%$.

The temperature dependent susceptibility (χ-T) were measured in an argon atmosphere (the flow rate is 50 ml/min) at a frequency of 976 Hz from room temperature up to 700 ℃ and back to room temperature using a MFK1-FA Kappabridge equipped with a CS-3 high-temperature furnace. The susceptibility of each sample was corrected for background (furnace tube correction) using the CUREVAL 8.0 program .

Hysteresis loops and first-order reversal curve (FORC) diagrams were measured by vibrating sample magnetometer (VSM3900) to a maximum applied field of 1 T. Hysteresis parameters, including the saturation magnetization (M_s), saturation remanent magnetization (M_{rs}), and coercivity (B_c), were obtained after subtracting the paramagnetic contribution. The remanence coercivity (B_{cr}) was obtained by demagnetizing samples from +1 T back to -1 T. The hysteresis ratios M_{rs}/M_s vs. B_{cr}/B_c were used to construct a Day plot .

The FORC diagrams were measured with the averaging time of 200 ms and produced using FORCinel software (Harrison and Feinberg, 2008). The total of 18 samples were used for detailed iron oxide analyses, including 2 samples from each natural dust source with modal χ_{lf} values, 4 dustfall samples and 2 street dust samples with high χ_{lf} and low χ_{lf}, and the 2 samples of vehicle exhausts and fly ashes.

The magnetic components of these representative samples were separated from the bulk samples using a 1 T magnet

sealed in a polyethylene bag. To confirm their mineral, morphological and elemental characteristics, direct observations and measurements of the samples and their extracted magnetic particles were performed using a ZEISS EVO-18 Scanning Electron Microscopy (SEM), equipped with Bruker XFlash 6130 Energy Dispersive Spectroscopy (EDS). Samples were mounted on SEM stub with double-sided carbon tape and then coated with thin gold film. The specified resolution of the SEM was < 5 nm. The EDS detector is capable of detecting elements with atomic numbers ≥5 and the detection sensitivity can reach 0.1 wt%. Bulk samples and magnetic extracts were characterized by randomly selecting 3-4 fields of view and examining all the particles observed within the selected fields. All the measurements were made at the Institute of Earth Environment, Chinese Academy of Sciences, Xi'an.

3 Results

3.1 Magnetic mineralogy

χ-T is used to identify magnetic mineral composition. All the χ-T heating curves (Fig. 3a-f) are characterized by a major susceptibility decrease at 580 ℃, i.e. the Curie temperature of magnetite, which pinpoint magnetite as the major contributor to χ. All the samples are irreversible with cooling paths above heating trajectories due to the neoformation of magnetite (Jordanova et al., 2004; Kim et al., 2009). The χ-T heating curves of the vehicle exhausts displays a decreasing χ between 580 and 700 ℃ (Fig. 3b), suggesting the presence of hematite.

All samples have similar slightly wasp-waisted hysteresis loops (Fig. 3g-l). Their magnetic saturation was generally reached at a magnetic field of about 300 mT. This is a clear indication of the predominance of low coercivity ferrimagnetic minerals in all samples.

3.2 Hysteresis properties

The Day plot and FORC diagram are powerful methods to identify the domain state distribution of magnetic materials (Day et al., 1977; Dunlop 2002a, b; Pike et al., 1999; Roberts et al., 2000). All the samples agree well with single-domain (SD) + multi-domain (MD) admixture curves in the pseudo-single-domain (PSD) range of the Day plot (Fig.4 a). The FORC

diagrams for street dust (Fig.4 d), and anthropogenic pollutant (Fig.4 e) have divergent contours that are characteristic of MD grains. The FORC diagram for natural surface sediments (Fig.4 a) seems to be characteristic of PSD/MD behavior, whose outer contours display divergent pattern and inner contours are somewhat less divergent . The FORC distributions of atmospheric dustfall (Fig.4 b) appear to have a mixed set of contours. The outer contours have a divergent pattern that would be expected for MD particles, while the inner contours close about a central peak represent SD grains.

3.3 Spatial and temporal variation of χ

Magnetic susceptibilities of all bulk samples were measured to estimate concentrations of magnetic minerals, which are largely controlled by concentrations of ferromagnetic minerals (Dunlop et al., 1997; Evans et al., 2003; Liu et al., 2012). χ_{fd} is sensitive to the superparamagnetic (SP) component. There are virtually no SP grains when χ_{fd} is < 2 %, while a mixture of SP and coarser grains is indicated with χ_{fd} in the range of 2-10% (Dearing et al. 1994). The χ_{lf} of the surface sediments varies from 7.1 - 88.9×10^{-8} m^3 kg^{-1} (Fig. 5a), while their χ_{fd} values range from 0.4 - 11.5 % (Fig. 5b). Both χ_{lf} and χ_{fd} exhibit a distinctive distribution pattern in different sources. In the TD, χ_{lf} varies from 12.5 - 40.3×10^{-8} m^3 kg^{-1}, with a unimodal distribution peaking at around 20 - 30×10^{-8} m^3 kg^{-1} (Fig. 5a), while χ_{fd} ranges from 3.0 - 11.5 % (Fig. 5b). χ_{lf} in the NCD is also unimodally distributed, ranging from 12.5 - 40.3×10^{-8} m^3 kg^{-1} with peak values at around 30 - 40×10^{-8} m^3 kg^{-1} (Fig. 5a), while χ_{fd} varies from 0.4 - 7.2% (Fig. 5b). In the MG, χ_{lf} ranges from 19 - 72.4×10^{-8} m^3 kg^{-1}, with a bimodal distribution peaking at around 30 - 40×10^{-8} m^3 kg^{-1} and 50 - 60×10^{-8} m^3 kg^{-1} (Fig. 5a), while χ_{fd} varies from 1.8 - 7.5 % (Fig. 5b). In the TP, χ_{lf} has a multimodal distribution in the range of 7.1 - 88.9×10^{-8} m^3 kg^{-1} with the highest peak at around 10 and 20×10^{-8} m^3 kg^{-1} (Fig. 5a), while χ_{fd} varies from 0.7 - 8.9 % (Fig. 5b). Different distribution patterns of χ_{lf} indicate that the assemblage of magnetic minerals in the NCD and TD may differ from those in the MG and TP.

The average χ_{lf} and χ_{fd} values of natural surface sediments are 32.9×10^{-8} m^3 kg^{-1} and 4.8 %, respectively. Average χ_{lf} in individual sources shows a decreasing trend from the MG (46.8×10^{-8} m^3 kg^{-1}), to NCD (38.4×10^{-8} m^3 kg^{-1}) and TP (29.6×10^{-8} m^3 kg^{-1}), and then to TD (23.6×10^{-8} m^3 kg^{-1}). The mean values of χ_{fd} in different natural sources show a decreasing trend of SP component from the TD (6.9 %) to MG (5.1 %) and TP (4.6 %), and then to NCD (2.5 %).

The χ_{lf} and χ_{fd} values of urban dust samples, including the street dust and atmospheric dustfall, vary from 90.4 -

1080.7×10^{-8} m^3 kg^{-1} (Fig. 5c), and from 0.8 - 10 % (Fig. 5d), respectively. However, the χ_{lf} values of the street dust (239.5 - 1080.7×110^{-8} m^3 kg^{-1}, mean 524.8×10^{-8} m^3 kg^{-1}) are higher than those of the atmospheric dustfall (90.4 - 972.2×10^{-8} m^3 kg^{-1}, mean 390.8×10^{-8} m^3 kg^{-1}). χ_{fd} ranges from 3.4 - 10.0 % (mean 6.1 %) for the street dust (Fig. 5d), and from 0.8 - 9.0 % (mean 5.4 %) for the atmospheric dustfall (Fig. 5d). Low χ_{lf} (< 500×10^{-8} m^3 kg^{-1}) occurs in the Ecological District, Han Chang'an city ruins Park, and Cultural District, while samples with intermediate χ_{lf} values (500 - 800×10^{-8} m^3 kg^{-1}) are from the moderately developed Industrial District and the periphery of the Commercial District. In contrast, the central areas of the Industrial District and the Commercial District (particularly the area of high traffic density at the Bell Tower) are characterized by relatively high χ_{lf} values (> 800×10^{-8} m^3 kg^{-1}). χ_{lf} of atmospheric dustfall from XA1 and XA2 exhibit significant and consistent seasonal variations (Fig. 6). The lowest (highest) χ_{lf} values correspond to highest (lowest) dust flux in spring (autumn). The frequency distributions of χ_{lf} for the street dust and atmospheric dustfall are unimodal with peaks at around 500 - 600 and 300 - 400×10^{-8} m^3 kg^{-1}, respectively (Fig. 5c).

The representative anthropogenic pollutants, i.e. the vehicle exhausts, fly ashes, and nearby street dust at the Bell Tower and thermal power plant, have high χ_{lf} (537.9 - 925.7×10^{-8} m^3 kg^{-1}) and χ_{fd} (8.5 - 11.1 %). The χ_{lf} and χ_{fd} of vehicle exhausts (925.7×10^{-8} m^3 kg^{-1}, 11.1 %) and fly ashes (770.0×10^{-8} m^3 kg^{-1}, 9.4 %) are higher than the mean values of street dust (524.8×10^{-8} m^3 kg^{-1}, 6.1 %) and atmospheric dustfall (390.8×10^{-8} 10^{-8} m^3 kg^{-1}, 5.4 %).

3.3 Morphology and mineralogy of the dust samples

To determine the mineralogical characteristics, more than 40 images were obtained randomly of the representative bulk samples. For comparison, images were obtained for various types of particles at the same magnification. The morphologies and mineral compositions of representative bulk samples of the natural surface sediments, street dust, and atmospheric dustfall with low and high $\chi_{lf,}$ are illustrated in Fig. 7. The particles are typically angular and irregularly shaped in the surface sediments, with a broad size range (around 1 - 100 μm). Based on the EDS analysis for each particles of the selected field, clay minerals, quartz, calcite, dolomite and magnetic grains (Fig. 7a) were clearly identified (Welton et al., 2012).

The SEM-DES analysis shows that the morphology and composition of the particles in the street dust are complex and heterogeneous. Three categories of particles can be morphologically differentiated, including irregular and aggregate mineral

particles, spherical particles, and anomalous particles with poriferous and loose structure (Fig. 7b). Particles with irregular shapes are mainly minerals and commonly present in street dust samples. Compared to the natural surface sediments, the grain size of mineral particles in the street dust is finer, and mostly ranges from 1 - 50 μm, with some up to 80 μm. Spherical particles are mainly amorphous silicon-aluminum and iron-rich spheres, whose grain size varies mostly from 1 - 20 μm with some up to 50 μm. There are a small number of anomalous particles with diameters of 10 - 100 μm.

The morphology and mineral composition of atmospheric dustfall are similar to those of the street dust, except that atmospheric dustfall with low χ_{lf} has a higher content of irregularly-shaped detrital minerals (Fig. 7c), while that with high χ_{lf} contains more spherical and anomalous particles (Fig. 7d).

3.4 Elemental compositions of mineral particles

Since the elemental compositions of mineral particles can be clearly distinguished using SEM-EDS analysis (Blanco et al., 2003; Barbara et al., 2006), a street dust sample dominated by anthropogenic inputs, which has the highest χ_{lf} in the street dust samples, was selected for analysis. A field of view is shown in Fig. 8. The various mineral particles exhibit distinct chemical compositions. The platy aggregates (labeled a) with high levels of Si and Al, and low levels of K, Ca, Mg and Fe are clay minerals composed of crystalline sheet-structure silicates with a small particle size (Fig. 8a). The angular and sharp-edged particle (labeled b) with high Si and O is quartz (Fig. 8b). The angular particle consisting of Si, Al, and K is potassium feldspar (Fig. 8c). Particles with the high levels of Ca and Mg are calcite (Fig. 8d) and dolomite (Fig. 8e).

The irregular particles (labeled f) which are abundant in Fe are identified as magnetic grains (Fig. 8f), although some of the particles show low levels of crustal elements, including Si, Al, Ca, and K. Two types of spheres were observed. One (labeled g) is an amorphous alumino-silicate particle (Fig. 8g) with predominant Si and Al and lesser amounts of K, Mg, Na and Ti. The other (labeled h) is an iron-rich sphere (Fig. 8h), which is mainly composed of Fe. These particles exhibit various surface textures. In addition, almost all particles contain O and C.

4 Discussion

4.1 Contributions of local anthropogenic sources estimated by dust flux and χ_{lf}

On the bivariate-plot of χ_{lf} vs. χ_{fd}, atmospheric dustfall is intermediate between the surface sediments and street dust (Fig.9b), implying that atmospheric dustfall is a mixture of distal natural dust and local anthropogenic dust, but much closer to the latter. The local anthropogenic contribution (LC) is mainly derived from local stable and sustained pollutant sources, including vehicle emissions and fly ashes. Considering that natural dust comes primarily from natural dust sources with a minor local soil contribution (Wang et al., 2004; Ginoux et al., 2012), we attribute the natural contribution entirely to the distal natural dust.

The dust flux background can be taken as the average input from the end member of LC. The time-dependent background estimation was calculated using:

$$x(i)_{bg} = \mathrm{MED}_{j=i-k}^{j=i+k}\left(x(j)\right), \quad (2)$$

$i=k+1,\ldots, n-k$, $x(i)_{bg}$ is the background of $x(i)$ at time $t(i)$. $\mathrm{MED}_{j=i-k}^{j=i+k}\left(x(j)\right)$ is the running median with window points of $2k+1$ ($k \leqslant (n-1)/2$) (Härdle and Steiger, 1995); cross-validation can be used to choose k. We used two such criterions: median criterion (Zhen and Yan, 1988) and L_1-norm (Marron, 1987):

$$CV_m(k) = \mathrm{median}\left\{\left|x(i) - \mathrm{MED}_{j=i-k,i\neq i}^{j=i+k}\left(x(j)\right)\right|\right\}, \quad (3)$$

$$CV_1(k) = \left[\sum_{i=1}^{n}\left|x(i) - \mathrm{MED}_{j=i-k,j\neq i}^{j=i+k}\left(x(j)\right)\right|\right] / n, \quad (4)$$

where $\mathrm{MED}_{j=i-k,\ j\neq i}^{j=i+k}\left(x(j)\right)$ is the delete-one background estimate. The cross-validation functions are to measure the average performance of the delete-one estimate to predict the observation $x(i)$. Optimal k values should minimize $CV_m(k)$ or $CV_1(k)$ (Mudelsee, 2006).

Through the cross-validation calculation on the dust flux series of atmospheric dustfall, we found that cross-validated number of window width (Eq. (3)) is k =19. On this basis, we calculated the monthly LC using the ratio of monthly background and total dust flux as the following:

$$LC_{flux} = x(j)_{bg} / DF \times 100\%, \quad (5)$$

where LC_{flux} is the percentage of the monthly local anthropogenic contribution estimated by dust flux. Note that when the background is larger than the dust flux (Fig. 10), LC is taken to be 100%.

M_s of representative samples (Fig.3h-m) were measured to identify concentration of ferrimagnetic minerals. We found that the averaged values of M_s in different sources show a rising trend from the natural surface sediments (0.04 Am^2/kg) to atmospheric dustfall (0.81 Am^2/kg) and street dust (1.03 Am^2/kg), and then to anthropogenic pollutant (1.58 Am^2/kg), which correspond to the characteristics of averaged χ_{lf} in different sources. This indicates that the high χ_{lf} of urban dust is caused by the ferrimagnetic mineral from local anthropogenic source. In consequence, the LC contribution could also be estimated by the average χ_{lf} (25×10^{-8} m^3 kg^{-1}) of the surface sediments and local street dust (550×10^{-8} m^3 kg^{-1}). On this basis, we calculated the LC using the following equation:

$$LC_{\chi}=(\chi_m-25)/(550-25)\times100\%$$

where LC_{χ} is the percentage of the local contribution estimated by χ_{lf} , and χ_m is the monthly average χ_{lf} value in 10^{-8} m^3 kg^{-1}. Note that when χ_m is larger than the average χ_{lf} of the street dust, LC is taken to be 100%.

The LC_{flux} and LC_{χ} values have the same trend and show a distinctive seasonal pattern (Fig. 10a-b), with the maximum in autumn (92.4 %, 92.3%), followed by winter (90.8 %, 74.7 %), summer (83.5 %, 71 %), and spring (73.0 %, 53.1%). Both the LC_{flux} and LC_{χ} are the lowest in spring, implying that distant natural dust input makes a great contribution to atmospheric dustfall during this period.

The LC variation exhibits a similar seasonal pattern with χ_{lf}, but opposite trend to that of dust flux (Fig. 10a-b). This suggests that the major sources of atmospheric dustfall varied seasonally between the distant natural sources in spring and local anthropogenic sources in other seasons. In spring, dust is emitted from the natural sources by strong winds, and after long-range transport it contributes to the elevated dust flux in Xi'an, and decreases the LC in atmospheric dustfall. However, from summer to winter, dust input from local anthropogenic sources is low and stable as indicated by the high LC.

4.2 Magnetic characteristics of anthropogenic particles

SEM-EDS analysis shows that the extracted magnetic particles from the street dust and atmospheric dustfall can be divided into detrital and anthropogenic types (Fig. 11a-c). Detrital particles are angular and characterized by relatively

smooth surfaces with Fe and O as the major elements and minor Ti (Fig. 11d), indicating the presence of magnetite, hematite, and titanomagnetite (Maher et al.,1991; Liu et al, 2015). Anthropogenic particles include angular particles with coarse surface textures, spherules, aggregates, and porous particles with complex internal structures. The major elements identified in these particles are Fe and O, which indicate the occurrence of magnetite or hematite, consistent with previously identified anthropogenic magnetic particles (Kim et al., 2007; Koukouzas et al., 2007; Maher et al., 2009). Minor concentrations of S, Zn, Cu and Cr were also observed in this type of particle, which is typically attributed to anthropogenic activities (Fig. 11d). The relatively weaker signal intensity of Fe in the EDS spectra of porous particles indicates a much lower Fe concentration (maximum less than 10 %), while their concentrations of Si, Al, Ca, Ti and Mn are higher.

SEM-EDS analysis shows that the morphology and concentration of magnetic materials in urban dust aerosols varied with sampling sites and over time. Among more than 20 images of analyzed magnetic extracts from urban dust samples, angular particles with coarse surface textures were the most frequently observed (> 50 %, some up to 80 %), with a wide range of grain size (1 - 100 μm). Spherules were also commonly observed in all samples, ranging from 10 - 40 %, mainly with diameters from 10 - 30 μm. The aggregates with diameters of 5 - 30 μm account for less than 10 %. Detrital particles, characterized by smooth surfaces, range from 1 - 5 % and have small diameters (10 - 20 μm). Porous particles are the least observed magnetic particles (< 1 %) with diameters of 30 - 120 μm. The SEM-EDS data show that the morphology and concentration of magnetic particulates in atmospheric dustfall with high χ_{lf} values are similar to those of the street dust, whereas atmospheric dustfall with low χ_{lf} contains more angular-subangular magnetic particles of detrital origin.

4.3 Potential sources of anthropogenic magnetic particles

Anthropogenic magnetic particles in the urban environment are mainly derived from the combustion of fossil fuels (Flanders, 1994; Matzka and Maher, 1999; Muxworthy et al., 2001), vehicle emissions (Harrison et al., 1997b; Moreno et al., 2003; Diapoui et al., 2008; Pant et al., 2013; Maher et al., 2013), and industrial activities (Hanesch et al., 2003; Desenfant et al., 2004). To clarify potential sources, microscopic and elemental investigations of magnetic extracts from anthropogenic pollutants were performed using SEM-EDS. Compared with the magnetic particles in atmospheric dustfall (Fig. 12a-d), those from vehicle exhausts consist of only three types of particles, including angular particles with coarse surface textures,

spherules and aggregates (Fig. 12e-g), while all magnetic particle types in dustfall samples were identified in fly ashes (Fig. 12h-k). The EDS analysis showed that the major elements of the same three types of magnetic particles in vehicle exhausts and fly ashes are Fe and O, consistent with elemental features of those in atmospheric dustfall (Fig. 12l-n). This suggests that vehicle exhausts and fly ashes are the main pollutant sources of the dustfall. However, there are some differences in compositions of the minor elements in the three types of particles between vehicle exhausts and fly ashes. Angular particles with coarse surface textures from vehicle exhausts contain more S, Cr, Cu, Zn and Mn, while those from fly ashes have more Ca and Mn. Aggregates consist of more Cr, Zn and S in vehicle exhausts, whereas Ca and S are enriched in fly ashes. Spherules from vehicle exhausts contain higher amounts of heavy metals (Cr, Ni Mn and Zn), while those from fly ashes have higher Ca and Mn. Coarse-grained porous magnetic particles were only observed in fly ashes, which are relatively low in Fe and high in crustal elements (e.g. Si, Al, K, Ca, Mg, and Ti).

The EDS elemental data clearly indicate that the magnetic particles from vehicle exhausts contain higher concentrations of a greater range of elements from anthropogenic activities (S, Cr, Cu, Zn, Ni and Mn) than those from fly ashes, whose EDS spectra show a substantial peak of Ca. The χ_{lf} (925.7×10^{-8} m^3 kg^{-1}) and M_s ($2.5 Am^2/Kg$) values of vehicle exhausts are significantly higher than those of the fly ashes (769.9×10^{-8} m^3 kg^{-1} and $0.66 Am^2/Kg$), indicating a higher content of ferrimagnetic contaminants. In summary, the magnetic particles emitted by vehicle exhausts and thermal power plants can be distinguished by a combination of morphological and elemental characteristics, which indicates that SEM-EDS can be used to trace the sources of anthropogenic pollutants in Xi'an.

5 Conclusions

By comparing the magnetic properties of surface sediments in natural dust sources in East Asia and various urban dust samples in Xi'an, we found that distal natural dust and local anthropogenic dust have different magnetic, morphological and elemental characteristics. We take natural surface sediments as the representative of distal natural dust, background atmospheric dustfall and polluted street dust as representatives of local anthropogenic dust. Based on this end-member configuration, relative contributions of local anthropogenic sources to urban atmospheric dustfall can be quantitatively

estimated. The results show that local anthropogenic contributions decrease in spring and increase in other seasons, exhibit a similar seasonal pattern with χ_{lf}, but opposite trend to that of dust flux. This means that dominant anthropogenic magnetic signals were diluted by less magnetic natural dust input. Hence, the local contribution is reduced as a result of increasing natural dust flux in spring.

SEM-EDS analysis of urban dust indicates that magnetic particles produced by anthropogenic activities have distinct morphological and elemental characteristics. The anthropogenic particles exhibit angular, spherical, aggregate, and porous shapes, and contain distinctive marker elements such as S, Cr, Cu, Zn, Ni, Mn and Ca. The porous particles are likely derived from the thermal power plant, while others may be attributed to both vehicle exhausts and the thermal power plant. Our results suggest that magnetic signatures combined with morphological and elemental compositions can be used to quantitatively estimate the local and anthropogenic contributions to urban dust aerosols.

Acknowledgements. We thank Min Zhao and Hua Wang for the help in sample collection. We are also grateful for the help of Maojie Yang with SEM-EDS measurements, and Jan Bloemendal with language polishing. This work was supported by the National Key Research and Development Program of China (2016YFA0601902) and the Open Foundation of State Key Laboratory of Loess and Quaternary Geology (SKLLQG1631).

References

Adachia, K., and Tainoshob,Y.: Characterization of heavy metal particles embedded in tire dust, Environment International., 30, 1009-1017, https://doi.org/10.1016/j.envint.2004.04.004, 2004.

Blanco, A., De Tomasi, F., Filippo, E., Manno, D., Perrone, M. R., A. Serra, A., Tafuro, A. M., and Tepore, A.: Characterization of African dust over southern Italy, Atmos. Chem. Phys., 3, 2147-2159, https://doi.org/10.5194/acp-3-2147-2003, 2003.

Baddock, M. C., Strong C. L., Murray, P. S., and McTainsh, G. H.: Aeolian dust as a transport hazard, Atmos. Environ., 71, 7-14, https://doi.org/j.atmosenv.2013.01.042, 2013.

Barbara, G., Kutchko., and Kim, A. G.: Fly ash characterization by SEM-EDS, Fuel., 85, 2537–2544, https://doi.org/10.1016/j.fuel.2006.05.016, 2006.

Blaha, U., Sapkota, B., Appel, E., Stanjek, H., and Rosler, W.: Micro-scale grain-size analysis and magnetic properties of coal-fired power plant fly ash and its relevance for environmental magnetic pollution studies, Atmos. Environ., 42, 8389-8370, https://doi.org/10.1016/j.atmosenv.2008.07.051, 2008a.

Blaha, U., Appel, E., and Stanjek, H.: Determination of anthropogenic boundary depth in industrially polluted soil and semi-quantification of heavy metal loads using magnetic susceptibility, Environmental Pollution., 156, 278-289, https://doi.org/10.1016/j.envpol.2008.02.013, 2008b.

Bourliva, A., Papadopoulou, L., and Aidona, E.: Study of road dust magnetic phases as the main carrier of potentially harmful trace elements, Sci. Total Environ., 553, 380-391, https://doi.org/10.1016/j.scitotenv.2016.02.149, 2016.

Brunekreef, B., Holgate, S. T.: Air pollution and health, Lancet., 360, 1233-1242, https://doi.org/10.1016/S0140-6736(02)11274-8, 2002.

Chen, Y. S., Sheen, P. C., Chen, E. R., Liu Y. K., Wu, T. N., and Yang, C. Y.: Effects of Asian dust storm events on daily mortality in Taipei, Taiwan, Environmental Research., 95, 151-155, https://doi.org/10.1016/j.envres.2003.08.008, 2004.

Chow, J. C., Engerlbrecht, J. P., Freeman, N. C. G., Hashim, J. H., Jantunen, M., Michaud, J. -P., de Tejada, S. S., Watson, J. G., Wei, F., Wilson, W. E., Yasuno, M., and Zhu, T.: Chapter one: exposure measurements, Chemosphere., 49, 873-901, https://doi.org/10.1016/S0045-6535(02)00233-3, 2002.

Day, R., Fuller, M., Schmidt, V.A.: Hysteresis properties of titanomagnetites: grain-size and compositional dependence. Phys Earth Planet Inter., 13, 260–267,1977.

Dearing, J. A.: Environmental Magnetic Susceptibility, Chi Publishing, Kenilworth, UK, 1994.

Dearing, J. A., Hay, K. L., Baban, S. M. J., Huddleston, A. S., Wellington, E. M. H., and Loveland, P. J.: Magnetic susceptibility of soil: an evaluation of conflicting theories using a national data set, Geophys. J. Int., 127, 728-734, https://doi.org/10.1111/j.1365-246X.1996.tb04051.x, 1996.

de Miguel, E., Llamas, J.F., Chacón, E., Berg, T., Larssen, S., Røyset, O., and Vadset, M.: Origin and patterns of distribution of trace elements in street dust: unleaded petrol and urban lead, Atmos. Environ., 31, 2733-2740, https://doi.org/10.1016/S1352-2310(97)00101-5, 1997.

Desenfant, F., Petrovský, E., and Rochette, P.: Magnetic Signature of Industrial Pollution of Stream Sediments and Correlation with Heavy Metals: Case Study from South France, Water, Air, and Soil Pollution., 152, 297-312, https://doi.org/10.1023/B:WATE.0000015356.88243.f0, 2004.

Diapouli, E., Chaloulakou, A., Mihalopoulos, N., and Spyrellis, N.: Indoor and outdoor PM mass and number concentrations at schools in the Athens area, Environ. Monit. Assess., 136, 13−20, https://doi.org/10.1007/s10661-007-9724-0, 2008.

Dunlop, D. J., and Özdemir, Ö.: Rock magnetism: Fundamentals and Frontiers, New York: Cambridge univ Press., 1997.

Dunlop, D. J.: Theory and application of the Day plot (Mrs/Ms versus Hcr/Hc) 1. Theoretical curves and tests using titanomagnetite data. J. Geophys. Res., 107, 2076, https://doi.org/10.1029/2001jb000486, 2002a.

Dunlop, D.J.: Theory and application of the Day plot (Mrs/Ms versus Hcr/Hc) 2. Application to data for rocks,sediments, and soils. J. Geophys. Res ., 107, 2057, https://doi.org/10.1029/2001jb000487, 2002b.

Dzubay, T. G., and Mamane, Y.: Use of electron microscopy data in receptor models for PM-10, Atmos. Environ., 23, 467-476, https://doi.org/10.1016/0004-6981(89)90590-8, 1989.

Elser, M., Huang, R . J., Wolf, R., Slowik, J. G., Wang, Q., Canonaco, F., Li, G., Bozzetti, C., Daellenbach, K. R., Huang, Y., Zhang, R., Li, Z., Cao, J., Baltensperger, U., El-Haddad, I., and Prévôt, A.S. H.: New insights into $PM_{2.5}$ chemical composition and sources in two major cities in China during extreme haze events using aerosol mass spectrometry, Atmos. Chem. Phys., 16, 3207–3225, https://doi.org/10.5194/acp-16-3207-2016, 2016.

Evans, M. E., and Heller, F.: Environmental Magnetism: Principle and Application of Enviromagnetics, International Geophysics Series Volume 86, Academic Press., Amsterdam, 2003.

Feng, S.P., Liu, H. C., Zhang, N. N., Lin, H., Du, X. L., and Liu, Y. L.: Contamination assessment of copper, lead, zinc and chromium in dust fall of Jinan, NE China, Environ. Earth Sci., 66, 1881-1886, https://doi.org/10.1007/s12665-011-1412-2, 2012.

Finlayson-Pitts, B. J., Wingen, L. M., and Sumner, A. L., Syomin, D., and Ramazan, K.A.: The heterogeneous hydrolysis of NO2 in laboratory systems and in outdoor and indoor atmospheres: An integrated mechanism, Phys. Chem. Chem. Phys., 5, 223-242, https://doi.org/10.1039/B208564J, 2003.

Flanders, P. J.: Collection, measurement, analysis of airborne magnetic particulates from pollution in the environment, Journal of Applied Physics., 75, 5931-5936, https://doi.org/10.1063/1.355518, 1994.

Fleming, Z. L., Monks, P. S., and Manning, A. J.: Review: Untangling the influence of air-mass history in interpreting observed atmospheric composition, Atmospheric Research., 104-015, 1-39, https://doi.org/10.1016/j.atmosres.2011.09.009, 2012.

Ginoux, P., Prospero, J. M., Gill,T. E., Hsu, N. C., and Zhao, M.: Global-scale attribution of anthropogenic and natural dust sources and their emission rates based on MODIS Deep Blue aerosol products. Reviews of Geophysics., 50, https://doi.org/10.1029/2012RG000388, 2012.

Ginoux, P., Prospero, J.M., Torres, O., and Chin, M.: Long-term simulation of global dust distribution with the GOCART model: correlation with North Atlantic Oscillation, Environ. Model Softw., 19, 113-128, https://doi.org/10.1016/S1364-8152(03)00114-2, 2004.

Gomez, E. T., Sanfeliu, T., Jordan, M. M., Rius, J., and de la Fuente, C.: Geochemical characteristics of particulate matter in the atmosphere surrounding a ceramic industrialized area. Environmental Geology., 45, 536-543, https://doi.org/10.1007/S00254-003-0908-9, 2004.

Gorden, G. E.: Receptor models. Environ. Sci. Technol., 22, 1132-1142, https://doi.org/10.1021/es00175a002, 1988.

Gupta, A. K., Karar, K., and Srivastava, A.: Chemical mass balance source apportionment of PM10 and TSP in residential and industrial sites of an urban region of Kolkata, India, Journal of Hazardous Materials., 142, 279-287, https://doi.org/10.1016/j.jhazmat.2006.08.013, 2007.

Härdle, W., Steiger, W.: Algorithm AS 296: Optimal median smoothing, Journal of the Royal Statistical Society. Series C (Applied Statistics)., 44, 258-264, 1995.

Hanesch, M., Scholger, R., and Rey, D.:Mapping dust distribution around an industrial site by measuring magnetic parameters of tree leaves, Atmos Environ., 37, 5125-5133, https://doi.org/10.1016/j.atmosenv.2003.07.013, 2003.

Hanisch, F., and Crowley, J. N.: Heterogeneous reactivity of gaseous nitric acid on Al_2O_3, $CaCO_3$, and atmospheric dust samples: A Knudsen cell study, J. Phys. Chem. A., 105, 3096-3106, https://doi.org/10.1021/jp001254+, 2001.

Hansard, R., Maher, B. A., and Kinnersley, R.: Biomagnetic monitoring of industry-derived particulate pollution, Environmental Pollution., 159, 1673-1681, https://doi.org/10.1016/j.envpol.2011.02.039, 2011.

Hansard, R., Maher, B. A., and Kinnersley, R. P.: Rapid Magnetic Biomonitoring and Differentiation of Atmospheric Particulate Pollutants at the Roadside and around Two Major Industrial Sites in the U.K., Environ. Sci. Technol., 46, 4403-4410, https://doi.org/10.1021/es203275r, 2012.

Harrison, R. M., Smith, D. J. T., Piou, C. A., and Castro, L. M.: Comparative receptor modellion study of airborne particulate pollutants in Birminghan, Coimbra and Lahore, Atmos. Environ., 131, 309-3321, https://doi.org/10.1016/S1352-2310(97)00152-0, 1997a.

Harrison, R. M.; Deacon, A. R.; Jones, M. R.; and Appleby, R. S.: Sources and processes affecting concentrations of PM_{10} and $PM_{2.5}$ particulate matter in Birmingham (U.K.), Atmos. Environ., 31, 4103−4117, https://doi.org/10.1016/S1352-2310(97)00296-3, 1997b.

Harrison, R. J., Feinberg, J. M.: FORCinel: An improved algorithm for calculating first-order reversal curve distributions using locally weighted regression smoothing, Geochem. Geophys. Geosyst., 9, Q05016, https://doi.org/10.1029/2008GC001987, 2008.

Hoffmann, V., and Knab, M., and Appel, E.: Magnetic susceptibility mapping of roadside pollution, J. Geochem. Explor., 66, 313-26, https://doi.org/10.1016/S0375-6742(99)00014-X, 1999.

Huang, R. J., Zhang, Y., Bozzetti, C., Ho, K. F., Cao, J. J., Han, Y. M., Daellenbach, K. R., Slowik, J. G., Platt, S. M., Canonaco, F., Zotter, P., Wolf, R., Pieber, S. M., Bruns, E. A., Crippa, M., Ciarelli, G., Piazzalunga, A., Schwikowski, M., Abbaszade, G., Schnelle-Kreis, J., Zimmermann, R., An, Z. S., Szidat, S., Baltensperger, U., Haddad, I. E., and Prevot, A. S. H.: High secondary aerosol contribution to particulate pollution during haze events in China, Nature., 514, 218-222, https://doi.org/10.1038/nature13774, 2014.

Huang, X. D., Olmezi, I., Aras, N. K., and Gordon, G. E.: Emission of trace elements from motor- vehicles-potential maker elements and source composition profile, Atmos. Environ., 28, 1385-1391, https://doi.org/10.1016/1352-2310(94)90201-1, 1994.

Hunt, A., Jones, J., and Oldfield, F.: Magnetic measurements and heavy metals in atmospheric articulateres of anthropogenic origin, Sci. Total Environ, 33, 129-139, https://doi.org/10.1016/0048-9697(84)90387-5, 1984.

Jordanova, D., Hoffmann, V., and Febr, K. T.: Mineralmagnetic characterization of anthropogenic magnetic phases in the Danube river sediments (Bulgarian part), Earth planet. Sci. Lett., 30, 71–89, https://doi.org/10.1016/S0012-821X(04)00074-3, 2004.

Jordanova, D., Jordanova, N., and Petrov, P.: Magnetic susceptibility of road deposited sediments at a national scale-relation to population size and urban pollution, Environ. Poll. 189, 239-251, https://doi.org/10.1016/j.envpol.2014.02.030, 2014.

Kan, H., London, S. J., Chen, G., Zhang, Y., Song, G., Zhao, N., Jiang, L., and Chen, B.: Differentiating the effects of fine and coarse particles on daily mortality in Shanghai, China, Environment International., 33, 376-384, https://doi.org/10.1016/j.envint.2006.12.001, 2007.

Kardel, F., Wuyts, K., Mahe, B.A., and Samson, R.: Intra-urban spatial variation of magnetic particles: Monitoring via leaf saturation isothermal remanent magnetisation (SIRM), Atmos. Environ., 55, 111-120, https://doi.org/10.1016/j.atmosenv.2012.03.025, 2012.

Kim, W., Doh,S. J., Park, Y. H., and Yun, S. T.: Two-year magnetic monitoring in conjunction with geochemical and electron microscopic data of roadside dust in Seoul, Korea, Atmos. Environ., 41, 7627-7641, https://doi.org/10.1016/j.atmosenv.2007.05.050, 2007.

Kim, W., Doh, S. J., and Yu, Y. J.: Anthropogenic contribution of magnetic particulates in urban roadside dust, Atmos. Environ., 43, 3137-3144, https://doi.org/10.1016/j.atmosenv.2009.02.056, 2009.

Koukouzas, N., Hämäläinen, J., Papanikolaou, D., Tourunen, A., and Jäntti, T.: Mineralogical and elemental composition of fly ash from pilot scale fluidised bed combustion of lignite, bituminous coal, wood chips and their blends. Fuel., 86, 2186-2219, https://doi.org/10.1016/j.fuel.2007.03.036, 2007.

Lee, S. H., Murphy, D. M., Thomson, D. S., and Middlebrook, A. M.: Chemical components of single particles measured with Particle Analysis by Laser Mass Spectrometry (PALMS) during the Atlanta SuperSite Project: focus on organic/sulfate, lead, soot, and mineral particles. Journal of Geophysical Research: Atmospheres., 107, 4003, https://doi.org/10.1029/2000JD000011, 2002.

Lee, P. K., Choi, B. Y., and Kang, M. J.: Assessment of mobility and bio-availability of heavy metals in dry depositions of Asian dust and implications for environmental risk, Chemosphere., 119, 1411-1421, https://doi.org/10.1016/j.chemosphere.2014.10.028, 2015.

Li, G. J., Chen, J., Ji, J. F., Yang, J., and Conway, T. M.: Natural and anthropogenic sources of East Asian dust, Geology., 37, 727-730, http://doi.org/10.1130/G30031A.1, 2009.

Li, P., Perreau, K. A,, Covington, E., Song, C. H., Carmichael, G. R., and Grassian, V. H.: Heterogeneous reactions of volatile organic compounds on oxide particles of the most abundant crustal elements: surface reactions of acetaldehyde, acetone, and propionaldehyde on SiO_2, Al_2O_3, Fe_2O_3, TiO_2, and CaO, Journal of Geophysical Research: Atmospheres., 106, 5517-5529, https://doi.org/10.1029/2000JD900573, 2001.

Liu, Q. S., Roberts, A. P., Larrasoaña, J. C., Banerjee, S. K., Guyodo, Y., Tauxe, L., and Oldfield, F.: Environmental Magnetism: Principles and Applications, Reviews of Geophysics., 50, 1-50, https://doi.org/10.1029/2012RG000393, 2012.

Liu, Q. S., Sun, Y. B., Qiang, X. K., Tada, R., Hu, P.X., Duan, Z. Q., Jiang, Z. X., Liu, J. X., and Su, K.: Characterizing magnetic mineral assemblages of surface sediments from major Asian dust sources and implications for the Chinese loess magnetism, Earth, Planets and Space., 67, 61, https://doi.org/10.1186/s40623-015-0237-8, 2015.

Lu, X., Zhang, X., Li, L. Y., and Chen, H.: Assessment of metals pollution and health risk in dust from nursery schools in Xi'an, China, Environmental research., 128, 27-34, https://doi.org/10.1016/j.envres.2013.11.007, 2014.

Maher, B. A., Ahmed, I. A. M., Davison, B., Karloukovski, V., and Clarke, R.: Impact of Roadside Tree Lines on Indoor Concentrations of Traffic-Derived Particulate Matter, Environ. Sci. Technol., 47, 13737−13744, https://doi.org/10.1021/es404363m, 2013.

Maher, B. A.: Rain and dust: magnetic records of climate and pollution, Elements., 5, 229-34,http://dx.doi.org/10.2113/gselements.5.4.229, 2009.

Maher, B. A., Moore, C., and Matzka, J.: Spatial variation in vehicle-derived metal pollution identified by magnetic and elemental analysis of roadside tree leaves, Atmos. Environ., 42, 364-373, https://doi.org/10.1016/j.atmosenv.2007.09.013, 2008.

Maher, B. A., and Thompson, R.: Mineral magnetic record of the Chinese loess and paleosols, Geology., 19, 3-6, https://doi.org/10.1130/0091-7613(1991)019<0003:MMROTC>2.3.CO;2, 1991.

Maher, B. A.: Magnetic properties of modern soils and Quaternary loessic palaeosols: palaeoclimatic implications, Palaeogeogr. Palaeoclimatol. Palaeoecol., 137, 25-54, https://doi.org/10.1016/S0031-0182(97)00103-X, 1998.

Marron, J. S.: What does Optimal Bandwidth Selection Mean for Nonparametric Regression Estimation?, Department of Statistics, University of North Carolina at Chapel Hill, 1986.

Matzka, J., and Maher, B.A.: Magnetic biomonitoring of roadside tree leaves: identification of spatial and temporal variations in vehicle-derived particulates, Atmos. Environ., 33, 4564-4569, https://doi.org/10.1016/S1352-2310(99)00229-0, 1999.

Meza-Figueroa, D., De la O-Villanueva, M., and De la Parra, M. L.: Heavy metal distribution in dust from elementary schools in Hermosillo, Sonora, Mexico, Atmos. Environ., 41, 276-288, https://doi.org/10.1016/j.atmosenv.2006.08.034, 2007.

Moreno, E., Sagnotti, L., Dinares-Turell, J.,Winkler, A., and Cascella, A.: Biomonitoring of traffic air pollution in Rome using magnetic properties of tree leaves, Atmos. Environ., 37, 2967–2977, https://doi.org/10.1016/S1352-2310(03)00244-9, 2003.

Mudelsee, M.:Short note: CLIM-X-DETECT: A Fortran 90 program for robust detection of extremes against a time-dependent background in climate records, Computers & Geosciences., 32, 141-144, https://doi.org/10.1016/j.cageo.2005.05.010, 2006.

Muxworthy, A. R., Matzka, J., and Petersen, N.: Comparison of magnetic parameters of urban atmospheric particulate matter with pollution and meteorological data, Atmos. Environ., 35, 4379-4386, https://doi.org/10.1016/S1352-2310(01)00250-3, 2001.

Nel, A., Xia, T., Madler, L., Li, N.: Toxic potential of materials at the nanolevel, Science., 311, 622−627, https://doi.org/10.1126/science.1114397, 2006.

Pacyna, J. M., and Pacyna, E. G.: An assessment of global and regional emissions of trace metals to the atmosphere from anthropogenic sources worldwide, Environmental Reviews., 9, 269-298, https://doi.org/10.1139/a01-012, 2001.

Pant, P.; and Harrison, R. M.: Estimation of the contribution of road traffic emissions to particulate matter concentrations from field measurements: A review, Atmos. Environ., 77, 78-97, https://doi.org/10.1016/j.atmosenv.2013.04.028, 2013.

Pickrell, J. A., Erickson, L. E.,Klabunde, K. J.: Toxicity of inhaled nanomaterials, In Nanoscale Materials in Chemistry, 2nd ed., Klabunde, K. J., Richards, R. M., Eds.; John Wiley & Sons, Inc., Chapter 22, 729−769, https://doi.org/10.1002/9780470523674.ch22, 2009.

Pike, C. R., Roberts, A. P., Verosub, K. L.: Characterizing interactions in fine magnetic particle systems using first order reversal curves, J. Appl. Phys., 85, 6660–6667, https://doi.org/10.1063/1.370176, 1999.

Qian, Z. M., He, Q. C., Lin, H. M., Kong, L. L., Liao, D. P., Dan, J. J., Bentley, C. M., and Wang, B. W.: Association of daily cause-specific mortality with ambient particle air pollution in Wuhan, China, Environ. Res., 105, 380-389, https://doi.org/10.1016/j.envres.2007.05.007, 2007.

Qiao, Q. Q., Huang, B. C., Zhang, C. X., Piper, J. D. A., Pan, Y. P., and Sun, Y.: Assessment of heavy metal contamination of dustfall in northern China from integrated chemical and magnetic investigation, Atmos. Environ., 74, 182-193, https://doi.org/10.1016/j.atmosenv.2013.03.039, 2013.

Quayle, B. M., Mather, T. A., Witt, M. L. I., Maher, B. A., Mitchell, R., Martin, R. S., and Calabrese, S.: Application and evaluation of biomagnetic and biochemical monitoring of the dispersion and deposition of volcanically-derived particles at Mt. Etna, Italy, Journal of Volcanology and Geothermal Research., 191, 107-116, https://doi.org/10.1016/j.jvolgeores.2010.01.004, 2010.

Roberts, A. P., Pike, C. R., Verosub, K. L.: First-order reversal curve diagrams: a new tool for characterizing the magnetic properties of natural samples, J. Geophys. Res., 105, 28461–28475, https://doi.org/10.1029/2000JB900326, 2000.

Rubasinghege, G., and Grassian, V. H.: Photochemistry of adsorbed nitrate on aluminum oxide particle surfaces, J. Phys. Chem. A., 113, 7818-7825, https://doi.org/10.1021/jp902252s, 2009.

Salvador, P., Artíñano, B., Alonso, D. G., Querol, X., Alastuey, A.: Identification and characterisation of sources of PM10 in Madrid (Spain) by statistical methods, Atmospheric Environment., https://doi.org/10.1016/j.atmosenv.2003.09.070, 38, 435-447, 2004.

Stein, A. F., Draxler, R. R., Rolph, G.D., Stunder, B. J. B., Cohen, M.D., and Ngan, F.: NOAA's HYSPLIT atmospheric transport and dispersion modeling system, Bull. Amer. Meteror. Soc., 96, 2059-2077, https://doi.org/10.1175/BAMS-D-14-00110.1, 2015.

Sushil, S., and Batra, V. S.: Analysis of fly ash heavy metal content and disposal in three thermal power plants in India, Fuel., 85, 2676-2679, https://doi.org/10.1016/j.fuel.2006.04.031, 2006.

Spassov, S., Egli, R., Heller, F., Nourgaliev, D. K. and Hannam, J.: Magnetic quantification of urban pollution sources in atmospheric particulate matter, Geophys. J. Int., 159, 555-564, https://doi.org/10.1111/j.1365-246X.2004.02438.x, 2004.

Sun, J. M., Zhang, M. Y., and Liu, T. S.: Spatial and temporal characteristics of dust storms in China and its surrounding regions, 1960-1999: relations to source area and climate. J. Geophys. Res., 106, 10325-10334, http://doi.org/10.1029/2000JD900665, 2001.

Sun, Y. B., Chen, H. Y., Tada, R., Weiss, D., Lin, M., Toyoda, S., Yan, Y., and Isozaki, Y.: ESR signal intensity and crystallinity of quartz from Gobi and sandy deserts in East Asia and implication for tracing Asian dust provenance, Geochem. Geophys. Geosyst., 14, 2615-2627, https://doi.org/10.1002/ggge.20162, 2013.

Takeuchi, M., Deguchi, J., Sakai, S., and Anpo, M.: Effect of H_2O vapor addition on the photocatalytic oxidation of ethanol, acetaldehyde and acetic acid in the gas phase on TiO_2 semiconductor powders, Applied Catalysis B: Environmental., 96, 218-223, https://doi.org/10.1016/j.apcatb.2010.02.024, 2010.

Urbat, M., Lehndorff, E., and Schwark, L.: Biomonitoring of air quality in the Cologne conurbation using pine needles as a passive sampler—Part I: magnetic properties, Atmos. Environ., 38, 3781-3792, https://doi.org/10.1016/j.atmosenv.2004.03.061, 2004.

Usher, C. R., Al-Hosney, H., Carlos-Cuellar, S., and Grassion, V. H.: A laboratory study of the heterogeneous uptake and oxidation of sulfur dioxide on mineral dust particles, Journal of Geophysical Research: Atmospheres., 107, ACH 16-1-ACH 16-9, https://doi.org/10.1029/2002JD002051, 2002.

Valavanidis, A., Fiotakis, K., and Vlachogianni, T.: Airborne Particulate Matter and Human Health: Toxicological Assessment and Importance of Size and Composition of Particles for Oxidative Damage and Carcinogenic Mechanisms, Journal of Environmental Science and Health, Part C-Environmental Carcinogenesis and Ecotoxicology Reviews., 26, 339-362, https://doi.org/10.1080/10590500802494538, 2008,

Voukand, V. B., and Piver, W. T.: Metallic elements in fossil fuel combustion products: amounts and form of emissions and evaluation of carcinogenicity and mutagenicity, Environmental Health Perspectives., 47, 201-225, 1983.

Wang, G., Oldfield, F., Xia, D,S., Chen, F. H., Liu, X. M., and Zhang, W. G.: Magnetic properties and correlation with heavy metals in urban street dust: a case study from the city of Lanzhou, China, Atmos. Environ., 46, 289-98, http://dx.doi.org/10.1016/j.atmosenv.2011.09.059, 2012.

Wang, X., Dong, Z., Zhang, J., and Liu, L.: Modern dust storms in China: an overview, Journal of Arid Environments., 58, 559-574, https://doi.org/10.1016/j.jaridenv.2003.11.009, 2004.

Welton, J. E., SEM petrology Atlas. The American Association of Petroleum Geologists.,Tulsa,1984.

Wehner, B., Birmili, W., Ditas, F.,Wu, Z., Hu, M., Liu, X., Mao, J., Sugimoto, N., and Wiedensohler, A.: Relationships between submicrometer particulate air pollution and air mass history in Beijing, China, 2004-2006, Atmos. Chem. Phys., 8, 6155-6168, http://doi.org/10.5194/acp-8-6155-2008, 2008.

Wilson, W. E., Chow, J. C., Claibom, C., Fusheng, W., Engelbrecht, J., and Watson, J. G.: Monitoring of particulate matter outdoors, Chemosphere., 49, 1009-1043, https://doi.org/10.1016/S0045-6535(02)00270-9, 2002.

Wu, L. Y., Tong, S. R., Wang, W. G., Ge, M. F.: Effects of temperature on the heterogeneous oxidation of sulfur dioxide by ozone on calcium carbonate, Atmospheric Chemistry and Physics., 11, 6593-6605, https://doi.org/10.5194/acp-11-6593-2011, 2011.

Xie, S., Dearing, J. A., Bloemendal, J., and Boyle, J. F.: Association between the organic matter content and.magnetic properties in street dust, Liverpool, UK, Science of the Total Environment., 241, 205-214, https://doi.org/10.1016/S0048-9697(99)00346-0, 1999.

Yan, Y., Sun, Y., Ma, L., and Long, X,: A multidisciplinary approach to trace Asian dust storms from source to sink, Atmos. Environ., 105, 43-52, https://doi.org/10.1016/j.atmosenv.2015.01.039, 2015b.

Yan, Y., Sun, Y., Weiss, D., Liang, L. J., and Chen, H. Y.: Polluted dust derived from long-range transport as a major end member of urban aerosols and its implication of non-point pollution in northern China, Science of The Total Environment., 506, 538-545, https://doi.org/10.1016/j.scitotenv.2014.11.071, 2015a.

Zdanowicz, C., Hall, G., Vaive, J., Amelin, Y., Percival, J., Girard, I., Biscaye, P., and Bory, A.: Asian dustfall in the St. Elias Mountains, Yukon, Canada, Geochimica et Cosmochimica Acta., 70, 3493-3507, https://doi.org/10.1016/j.gca.2006.05.005, 2006.

Zhang, C. X., Qiao, Q. Q., Appe,l E., and Huang, B. C.: Discriminating sources of anthropogenic heavy metals in urban street dusts using magnetic and chemical methods, J. Geochem. Explor., 119-120, 60-75, https://doi.org/10.1016/j.gexplo.2012.06.014, 2012a.

Zhang, C. X., Erwin, A., and Qiao, Q. Q.: Heavy metal pollution in farmland irrigated with river water near a steel plant—magnetic and geochemical signature, Geophysical Journal International., https://doi.org/10.1093/gji/ggs079, 2012b.

Zhang, C. X., Qiao, Q. Q., Piper, J. D. A., and Huang, B. C.: Assessment of heavy metal pollution from a Fe-smelting plant in urban river sediments using environmental magnetic and geochemical methods, Environmental Pollution., 159, 3057-3070, https://doi.org/10.1016/j.envpol.2011.04.006, 2011.

Zhang, R., Wang, M., Zhang, X., and Zhu, G.: Analysis on the chemical and physical properties of particles in a dust storm in spring in Beijing. Powder Technology., 137, 77-82, https://doi.org/10.1016/j.powtec.2003.08.056, 2003.

Zheng, Z. G., Yang, Y.:Cross-validation and median criterion, Statistica Sinica., 8 , 907–921, 1998.

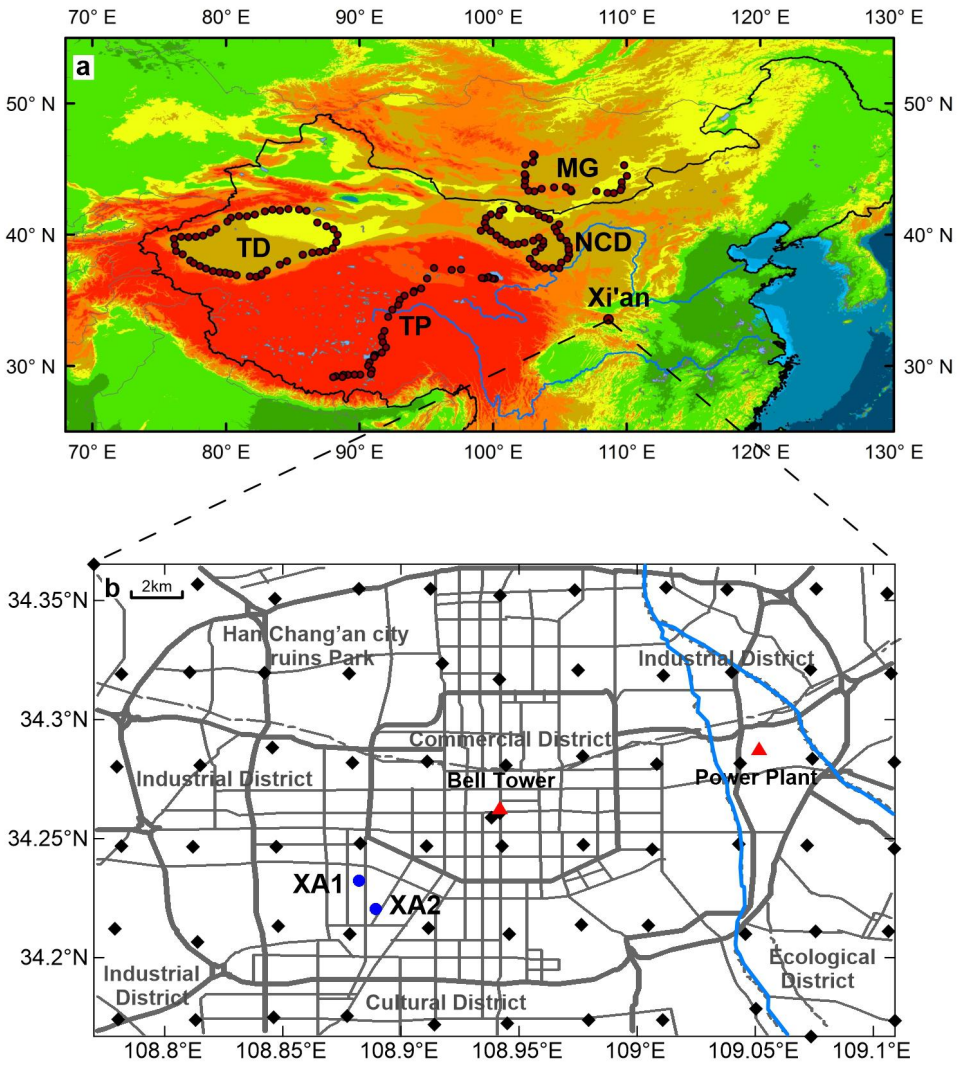

Figure 1. Locations of natural surface sediments (NSS) in the East Asian sources (a) and urban dust samples in Xi'an (b). NCD - northern Chinese deserts, MG - Mongolian Gobi, TD - Taklimakan Desert, and TP - Tibetan Plateau. Black diamonds are STD sampling sites; blue dots are samples of consecutive AD (XA1 at the Institute of Earth Environment, Chinese Academy of Sciences; XA2 at the Xinxinjiayuan residential community); red triangles are typical heavily-polluted sites, including the Bell Tower in an area of high traffic density, and the Baqiao thermal power plant.

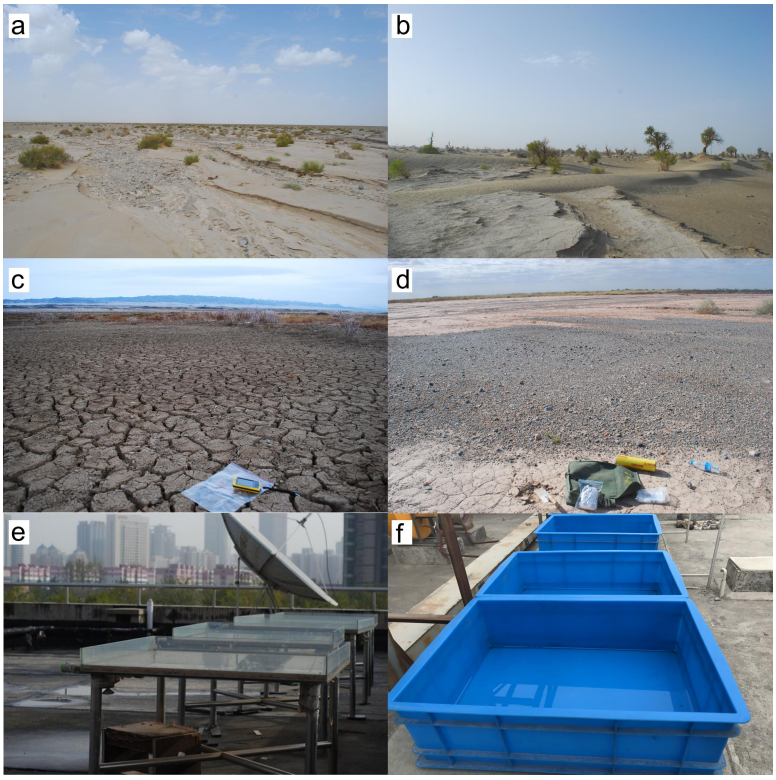

Figure 2. Sampling sites of NSS in a dry riverbed (a), desert margin (b), drainage depressions within sandy desert (c), and Gobi deserts (d), and AD at XA1 (e) and XA2 (f).

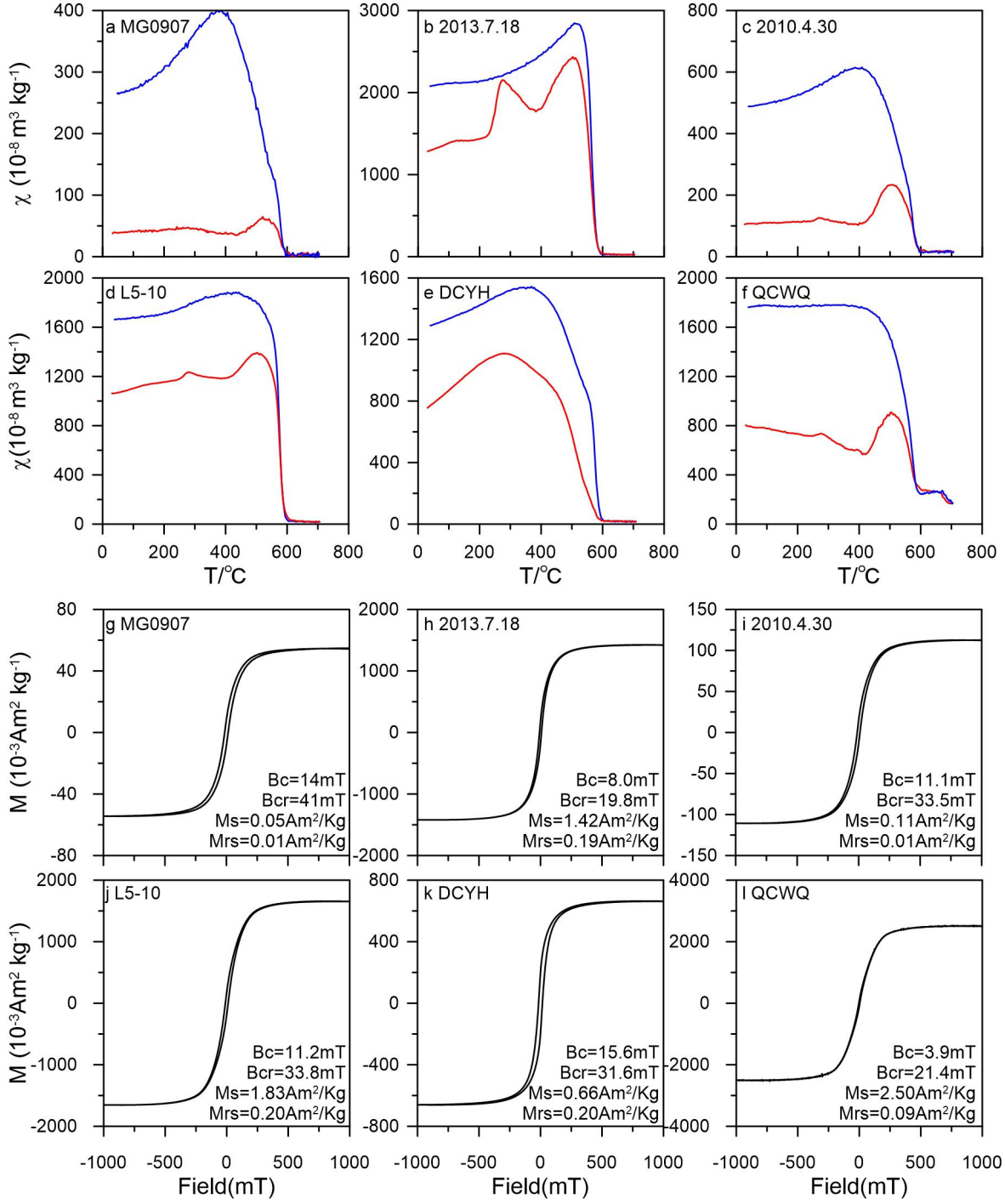

Fig 3. χ-T heating (red line) and cooling (blue line) curves (a-f) and magnetic hysteresis loops (g-l) of representative samples of NSS (MG0907), atmospheric dustfall (AD, 2013.7.18 and 2010.4.30), street dust (STD, L5-10) and anthropogenic pollutant (AP): fly ashes (DCYH) and vehicle exhausts (QCWQ).

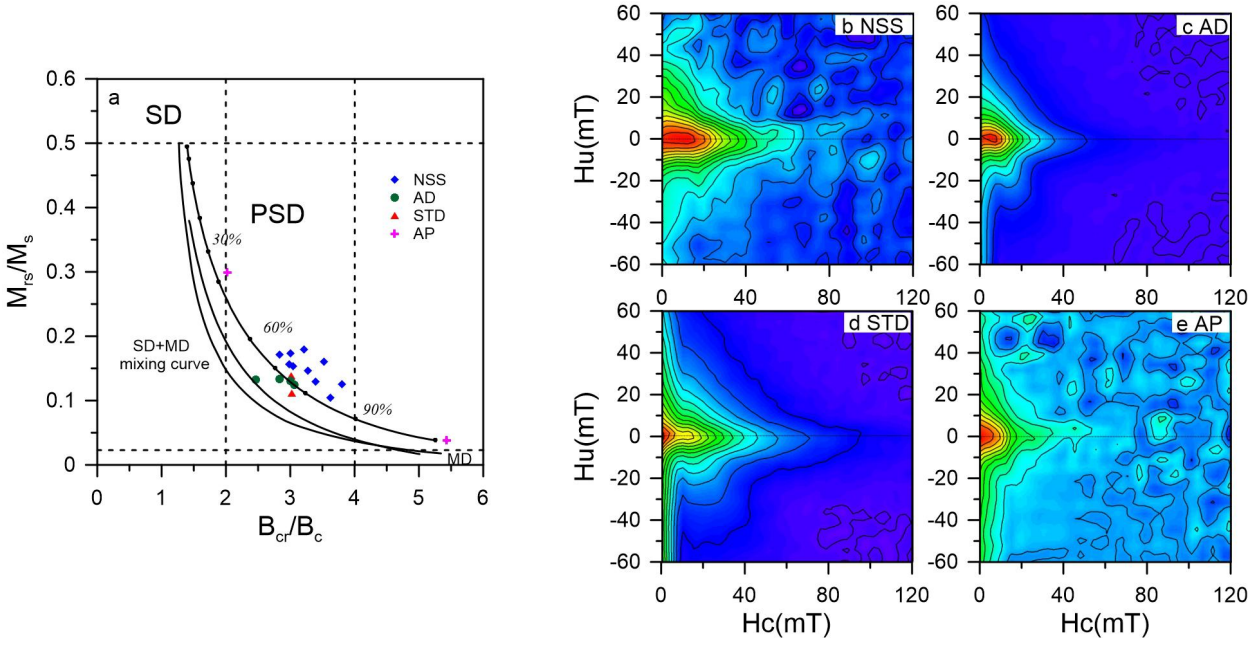

Fig. 4 (a) Day-plot of the ratios M_{rs}/M_s and B_{cr}/B_c for representative samples from NSS, AD, STD, and AP, grain size boundaries and the SD+MD matrix line are according to Dunlop (2002b). Percentages in the Day plot represent the concentrations of MD in the SD+MD mixture; (b-e) FORC diagrams for representative samples of NSS, AD, STD, and AP.

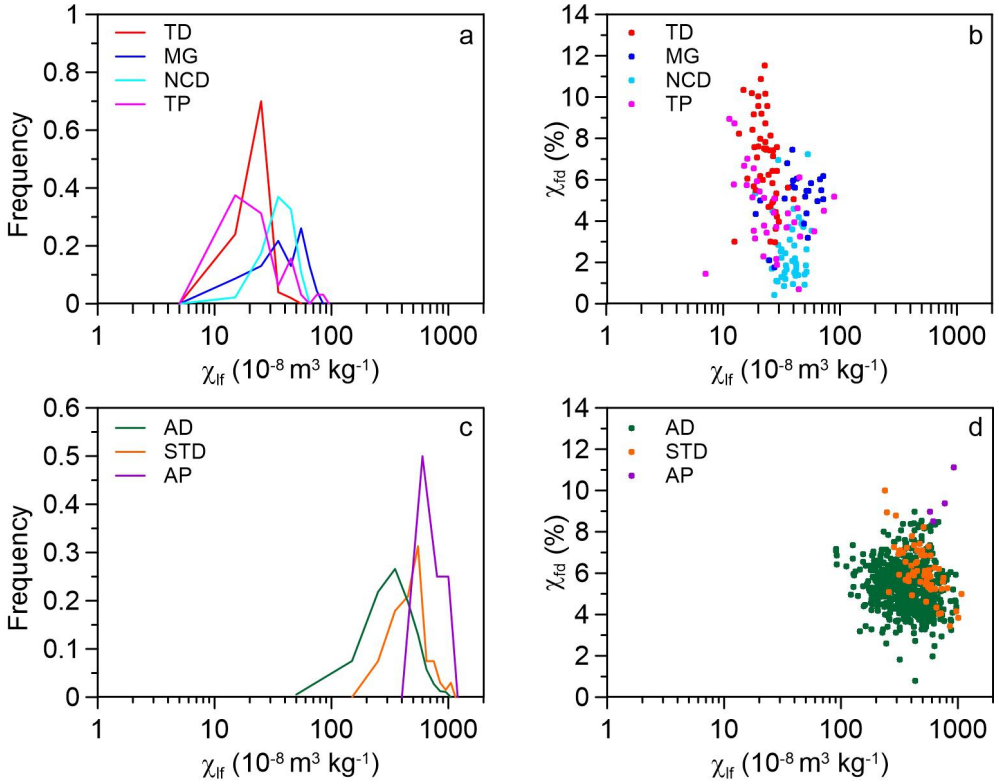

Figure 5. Frequency distribution of χ_{lf} and bivariate plots of χ_{lf} and χ_{fd} of NSS in each source (a, b) and urban dust aerosols (c, d), including AD, STD and AP. Frequency distribution statistics of χ_{lf} for NSS, AD and STD, and AP were generated using intervals of 10×10^{-8} m^3 kg^{-1}, 100×10^{-8} m^3 kg^{-1} and 200×10^{-8} m^3 kg^{-1} respectively.

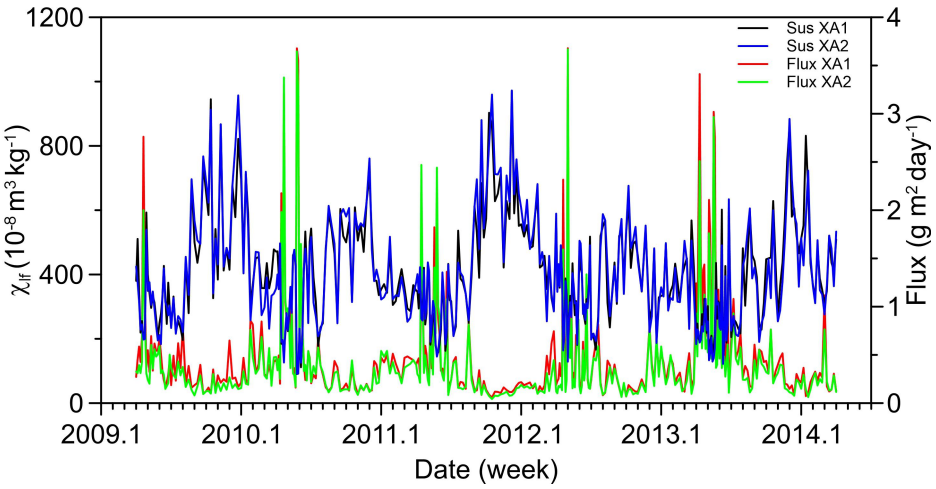

Figure 6. Time series of magnetic susceptibility and dust flux of AD at XA1 and XA2, from 2009 to 2014.

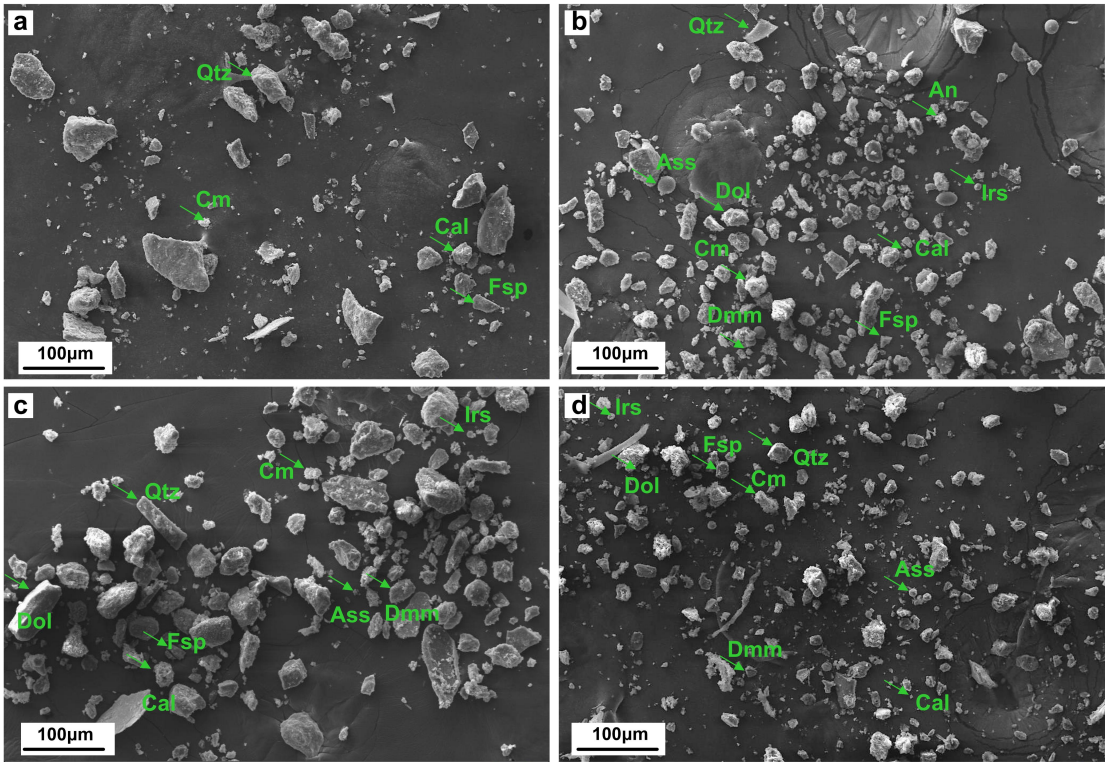

Figure 7. Morphology and mineralogy of representative samples of the NSS (a), STD (b), AD with low χ_{lf} (c) and high χ_{lf} (d). Qtz - quartz, Fsp - feldspar, Cal - calcite, Dol - dolomite, Cm - clay minerals, Dmm - detrital magnetic mineral, Irs - iron-rich sphere, Ass - aluminosilicate sphere, An - anomalous particles with a poriferous and loose structure.

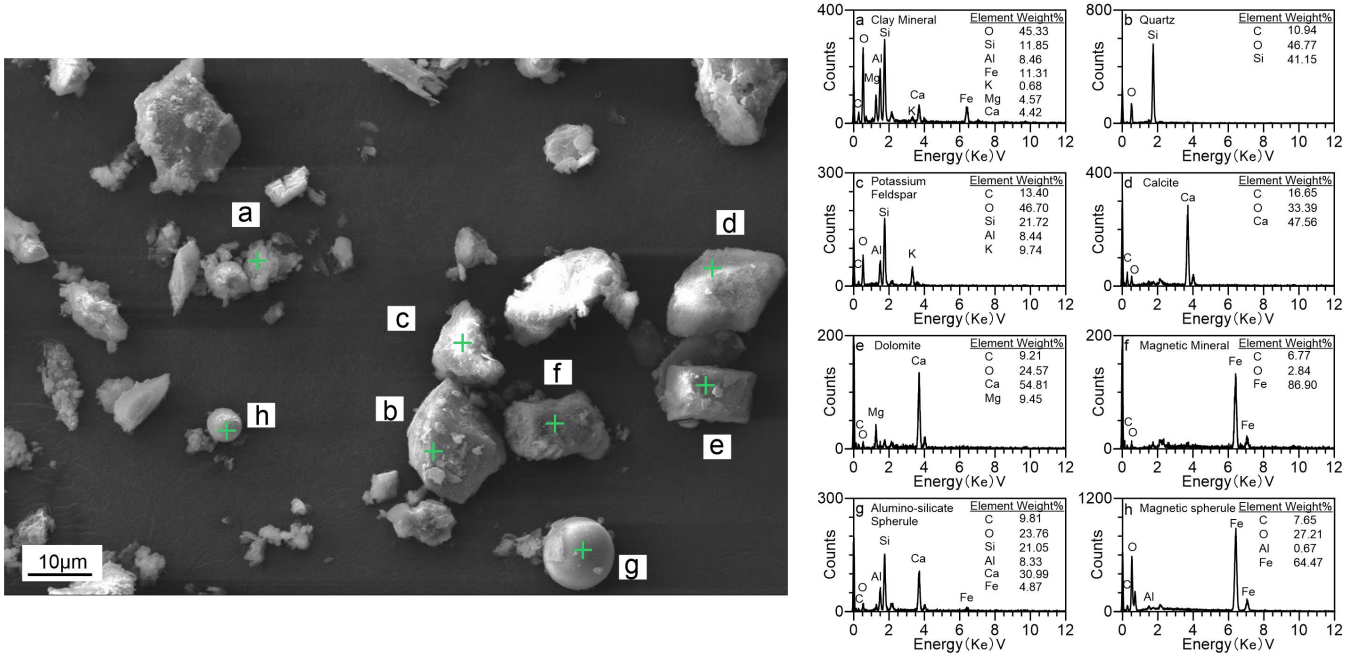

Figure 8. SEM photograph and elemental spectra for a typical sample of STD. In the subplots the green plus symbols denote the locations of the beam used in the EDS analysis.

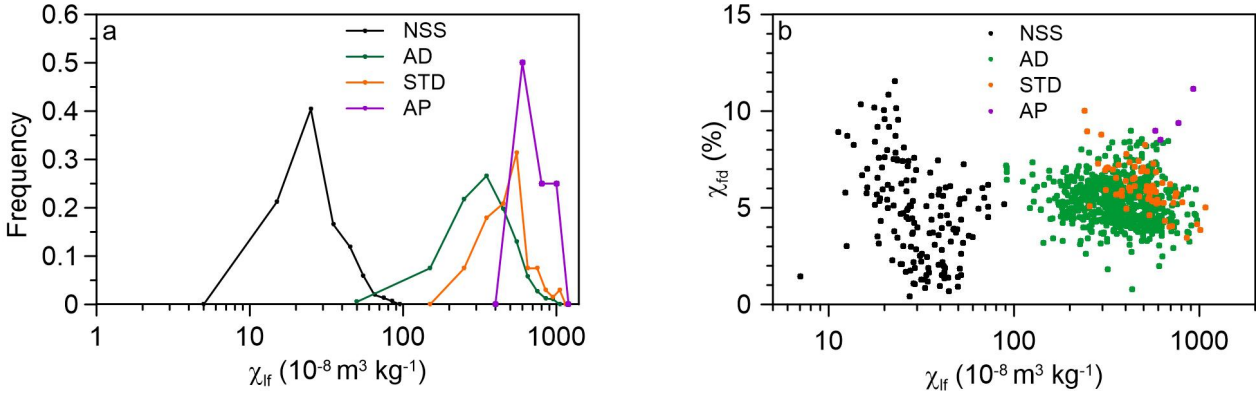

Figure 9. Frequency distributions of χ_{lf} (a) and bivariate-plots of χ_{lf} versus χ_{fd} (b) of NSS, STD, AD, and AP.

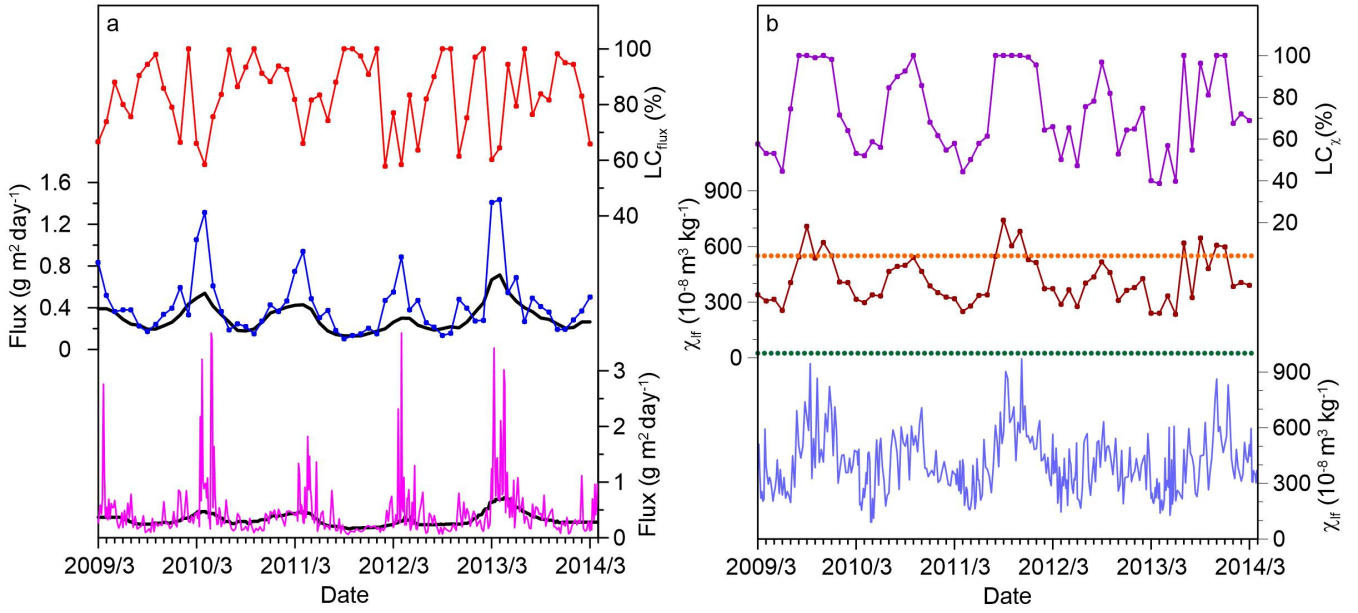

Fig. 10 The estimated local anthropogenic contributions by dust flux (a) and χ_{lf} (b). From bottom to top: (a) weekly dust flux (pink) and background estimate by the running median with a cross-validated number of window points (k=19) (black), monthly averaged dust flux (blue) and background (black), local contribution (red) estimate by dust flux at XA1; (b) weekly χ_{lf} values (light blue), averaged χ_{lf} values of natural distant dust (green dotted lines), monthly averaged χ_{lf} values (brown), averaged χ_{lf} values of local street dust (orange dotted lines) , local contribution (violet) estimate by χ_{lf} at XA1.

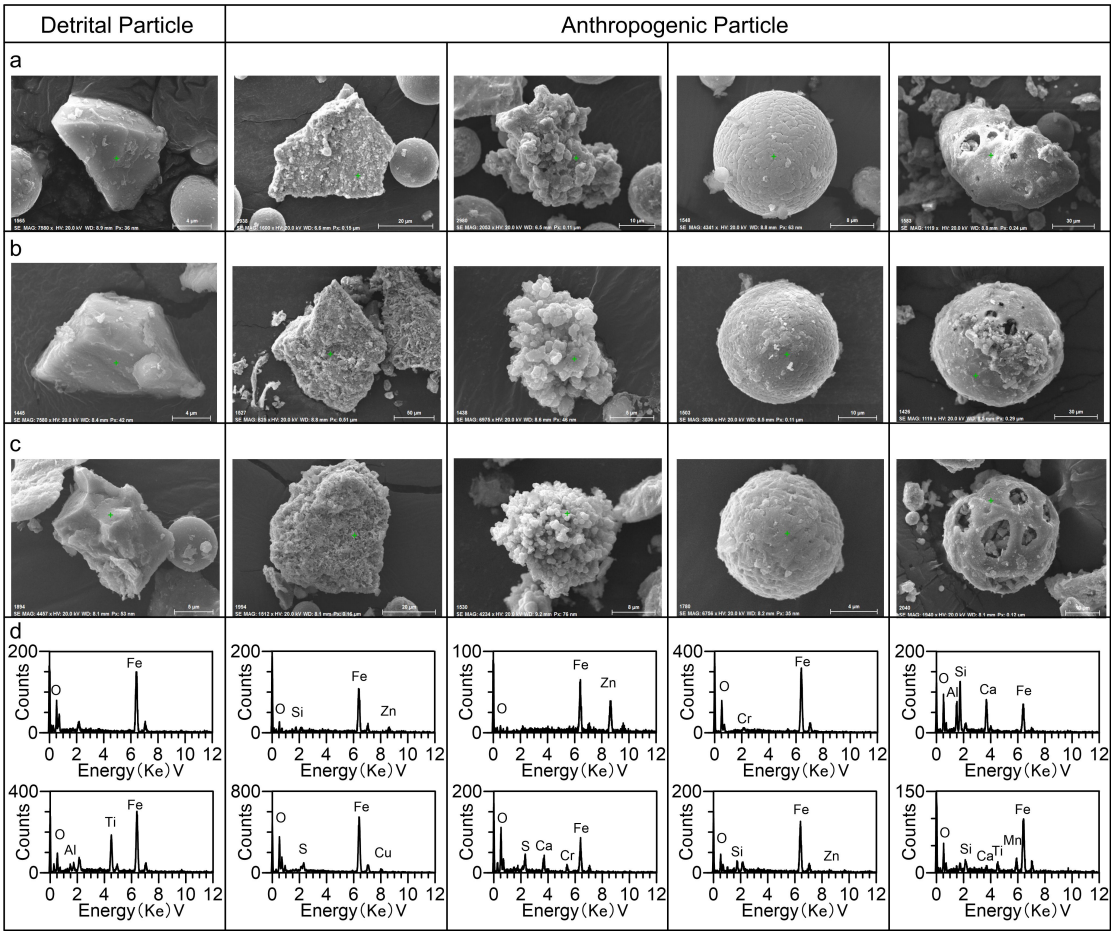

Figure 11. SEM images and typical elemental spectra (d) of magnetic extracts from STD(a), AD with high χ_{lf} (b) and low χ_{lf} (c). From left to right, the particle morphologies represent detrital particles with relatively smooth surfaces from natural source regions, and anthropogenic particles with angular shapes and coarse surface textures, aggregates, spherules, and porous feature.

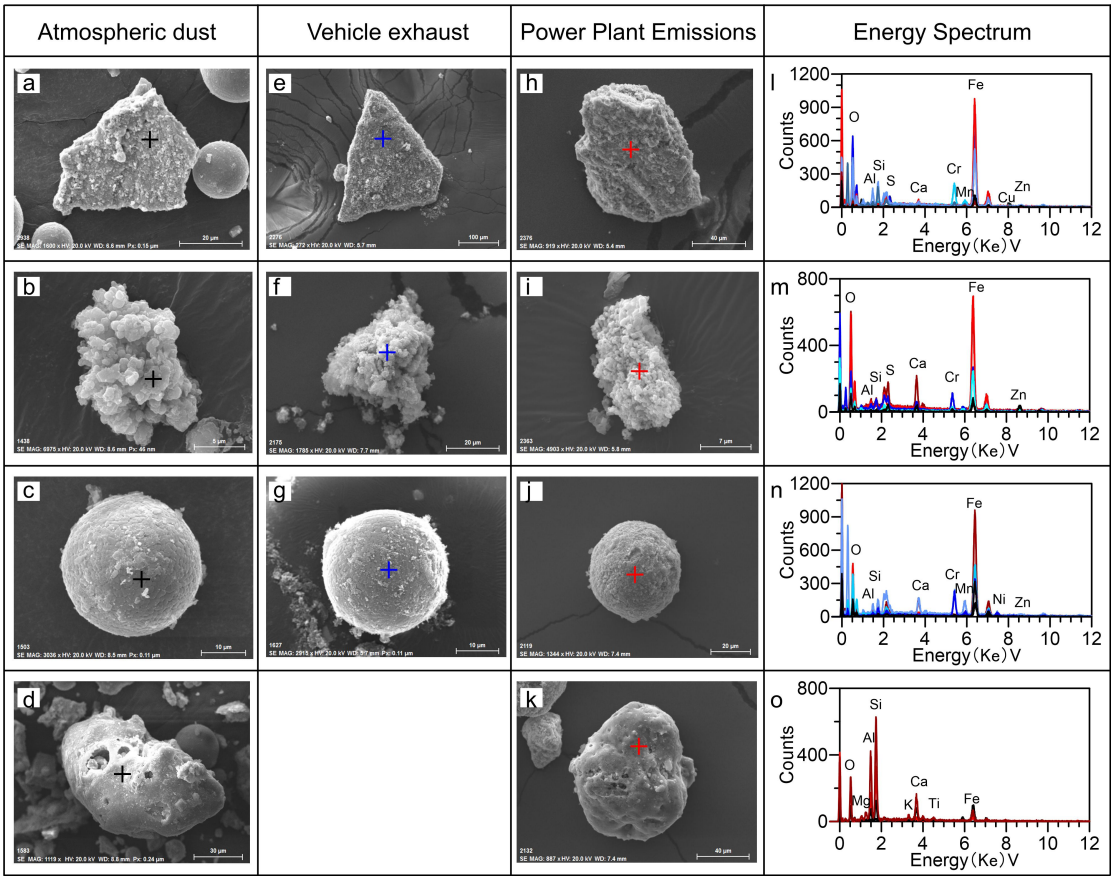

Figure 12. SEM images and elemental spectra of magnetic extracts from AD (a-d), vehicle exhausts (e-g) and fly ashes (h-k) . Black lines are elemental spectra of AD. Blue and red lines are elemental spectra for vehicle exhausts and fly ashes.